AFFIDAVIT

I declare that I have authored this thesis independently, that I have not used other than the declared sources/resources, and that I have explicitly indicated all material which has been quoted either literally or by content from the sources used. The text document uploaded to TUGRAZonline is identical to the present master‘s thesis dissertation.

Date

Signature

Acknowledgements

First of all, I would like to extend my sincerest thanks to my supervisor Karl Gruber, who was always supportive and encouraging. Be it about preparing presentations, experimental procedures or writing this thesis, if I was in need of assistance, I always knew I could turn to him. Simply put, I could not have wished for a better supervisor.

I would also like to thank Prashant Kumar. He was a kind and patient teacher, who poured his heart and soul into this project. He, as well as my office neighbour Altijana Hromic, could always be relied upon for scientific advice and moral support.

My thanks also go to Viktoria Reihofer, who coordinated the experiments with me and also contributed a big part of the experimental work.

Furthermore I would like to thank Silvia Wallner, who aided with the ITC experiments, Jakov Ivkovic who synthesized one of the inhibitors used in this project and Tea Pavkov-Keller for her great and reliable advice about crystallography in general and structure determination in particular.

I would also like to express my gratitude towards everyone else in the Strubi group for being so kind and welcoming.

Finally, I would like to thank my family for their unwavering support throughout my studies.

Abstract

Dipeptidyl Peptidase III (DPP III) is a zinc dependent aminopeptidase with a unique catalytic motif, which is able to hydrolyze a wide variety of bioactive substrates. It is suggested to play an important role in mammalian blood pressure regulation, pain modulation and in the later stages of protein turnover, yet its exact function is still largely unknown. Furthermore, DPP III was found to be a member of the human central proteome and overexpressed in certain types of cancer cells. In order to understand how DPP III is able to accommodate substrates of varying lengths, almost irrespective of their amino acid composition and to elucidate its exact catalytic mechanism, crystallographic studies were performed. In this thesis we present crystal structures of human inactive DPP III in complex with the synthetic inhibitor (S)-hydroxyethylene (SHE) and the hemorphin-like pentapeptide inhibitor IVYPW. Structures of hDPP III bound to in vitro substrates were also obtained and analysed in this project. We found that binding of a peptide induces a large domain motion, which forms the active site by bringing catalytic residues in close proximity to the ligand binding domain. Futhermore, we were able to confirm the presence of an anion-π interaction, which facilitates correct positioning of a catalytically important glutamic acid residue in the active site.

Keywords: dipeptidyl peptidase III, crystallographic studies, anion-π interaction, synthetic inhibitors

Zusammenfassung

Dipeptidyl Peptidase III (DPP III) ist eine metallabhängige Aminoprotease mit einem einzigartigen katalytischen Bindemotiv, welche in der Lage ist eine Vielfalt von bioaktiven Substraten zu hydrolysieren. Studien deuten an, dass DPP III in der Blutdruckregulation von Säugetieren, sowie im Schmerz-modulationssystem und im Proteinumsatz beteiligt ist. Weiters ist DPP III ein Mitglied des human central proteome und Überexpression des Enzyms konnte in bestimmten Krebsarten festgestellt werden. Die genaue Funktion von DPP III ist jedoch weitgehend unbekannt. Um zu analysieren wie DPP III in der Lage ist Substrate von stark variierender Länge und Zusammensetzung effektiv zu hydrolysieren, wurden kristallographische Studien durchgeführt. In der vorliegenden Arbeit präsentieren wir kristallographische Strukturen von humaner, inaktivierter DPP III in Komplex mit dem Pentapeptid IVYPW und dem synthetischen Inhibitor (S)-hydroxyethylene (SHE). Substratgebundene Strukturen wurden ebenfalls in diesem Projekt erhalten und analysiert. Durch Ligandenbindung wird eine Bewegung der Proteindomänen induziert, welche das aktive Zentrum formt, indem die katalytischen Reste in Kontakt mit der Substratbindestelle gebracht werden. Weiters konnten wir eine Anionen-π Interaktion feststellen, welche die korrekte Positionierung einer katalytischen Glutaminsäure im aktiven Zentrum unterstützt.

Schlüsselwörter: dipeptidyl peptidase III, Kristallographische Studien, Anionen-π Interaktion, Synthetische Inhibitoren

Table of contents

Affidavit **1**
Acknowledgements **2**
Abstract **3**
Zusammenfassung **4**
1. Introduction **6**
2. Materials and methods **11**
2.1 Site-directed mutagenesis and plasmid isolation 11
2.2 Protein expression and purification 13
2.3 Crystallization 16
2.4 Data collection and structure determination 18
2.5 Fluorescent activity assay 18
2.6 Isothermal titration calorimetry 19
3. Results **20**
3.1 Protein purification 20
3.2 Crystal structures 23
3. 2. 1 hDPP III in complex with IVYPW 26
3. 2. 2 hDPP III in complex with SHE 29
3.3 Fluorescent activity assay 33
3.4 Isothermal titration calorimetry 34
4. Discussion **36**
4.1 hDPP III in complex with synthetic inhibitors 39
4.2 hDPP III in complex with in vitro substrates 41
4. 2. 1 hDPP III in complex with Met-enkephalin and Leu-enkephalin 41
4. 2. 2 hDPP III in complex with angiotensin-II 44
4. 2. 3 hDPP III in complex with endomorphin-2 47
4.3 Anion - aromatic interaction 49
4.4 Proposed mechanism of catalysis 51
4.5 Conclusions 56
List of figures **58**
5. List of tables **60**
6. References **61**

1. Introduction

General information - Dipeptidyl peptidase III (DPP III) is a zinc dependent exopeptidase, with the capability of binding a large variety of oligopeptides and sequentially cleaving dipeptides from their amino termini. It belongs to the M49 family of metallopeptidases, who are characterized by their unique zinc binding motifs of HEXXGH and EEXRAE/D [1]. DPP III is capable of hydrolyzing peptides of varying length from four up to ten residues, almost irrespective of their amino acid composition [2]. Most notably, DPP III is able to degrade bioactive opioid peptides such as leu-enkephalin, met-enkephalin, valorphin and endomorphin-2. Due to this affinity for bioactive substrates, it has previously been characterized as Enkephalinase B [2,3]. In solution, DPP III is most likely present as a monomeric protein of 82 kDa, with a length of 737 amino acids [4]. Homologues of DPP III have been identified predominantly in the cytosol of several prokaryotic, as well as eukaryotic organisms [2].

Biological relevance - Hydrolysis of key proteins in the endocrinous and nervous system by DPP III would prevent interaction with their corresponding receptors, thereby inactivating downstream activity. Because DPP III is capable of degrading enkephalins at physiological pH value, it is implicated to be involved in pain modulation [5]. Furthermore, DPP III degrades angiotensin-II, which is a metabolite in the renin/angiotensin system (RAS), wherein it acts as a potent vasoconstrictor. Therefore, DPP III is also proposed to play a significant role in mammalian blood pressure regulation [2,6]. In addition to degrading bioactive peptides, studies also suggest DPP III to be involved in later stages of protein turnover and oxidative stress response [7]. It can also act as a post-proline cleaving enzyme, as evident by its ability to effectively hydrolyze substrates such as endomorphin-1 and endomorphin-2 [8]. DPP III was identified as a member of the human central proteome, which is a set of proteins abundantly and ubiquitously expressed in all human cell lines [33]. Studies have shown a significant increase in DPP III activity in malignantly transformed ovarian tissue cells and enhanced DPP III activity was directly correlated to the aggressiveness of the tumor. Therefore, DPP III is

proposed to be involved in pathophysiological conditions such as cancer as well [9].

Structural overview - Previously solved crystal structures of yeast DPP III from *Saccharomyces cerevisiae* (yDPP III) and human DPP III without ligand (Protein Data Bank codes 3CSK and 3FVY respectively) have given us a general overview of the enzymes structure. DPP III can be separated into an upper domain, consisting mostly of α-helices and a lower domain with mixed α-helices and β-sheets. The two domains are separated by a wide cleft of about 40 Å in length in the open structure [10]. The core region of the lower domain is formed by a 5 stranded β-sheet structure, which also houses the substrate binding site. A highly flexible helical loop between these domains serves as a hinge region [10]. Unbound hDPP III has been observed in an open, elongated conformation which guarantees accessibility to the substrate binding site, while hDPP III in complex with the synthetic hemorphin-like peptide tynorphin, has been observed in a closed, more globular conformation [11,14]. It has therefore been proposed, that hDPP III undergoes a large domain motion upon binding of a ligand molecule [11]. A comparison between the open, unbound structure and the closed structure in complex with tynorphin is depicted in figure 1.

Conserved motifs and zinc coordination - The M49 family of metallopeptidases is characterized by their novel **H**EXXG**H** and -E**E**XRAE/D conserved structural motifs. Both of which are located on the enzymes upper domain. The two histidine residues and the glutamic acid residue depicted in bold letters are involved in coordination of the catalytic zinc ion [12,13]. In yDPP III, the zinc ion is coordinated via His460 and His465 from the ^{460}HEXXGH^{465} consensus sequence and Glu517 from the ^{516}EECRA(E/D)^{521} sequence. In hDPP III, the zinc ion is coordinated via His450 and His455 from the ^{450}HEXXGH^{455} sequence, as well as Glu508 from the ^{507}EECRA(E/D)^{512} sequence [12]. Other well characterized members of the zinc metalloprotease superfamily, such as zincins or glucincin, contain an α-helical HEXXH zinc binding-motif. In members of the M49 family, the distance between the zinc coordinating His residues is extended by one additional residue. However, some members of family M49, notably from bacteria such as *Colwelia* possess the more common

HEXXH motif[15]. The second of these glutamic acid residues is replaced by aspartic acid in some members of the family. The two remaining glutamic acid residues from the EEXRAE/D motif are hydrogen bonded to the zinc coordinating histidine residues from the HEXXGH motif [10].

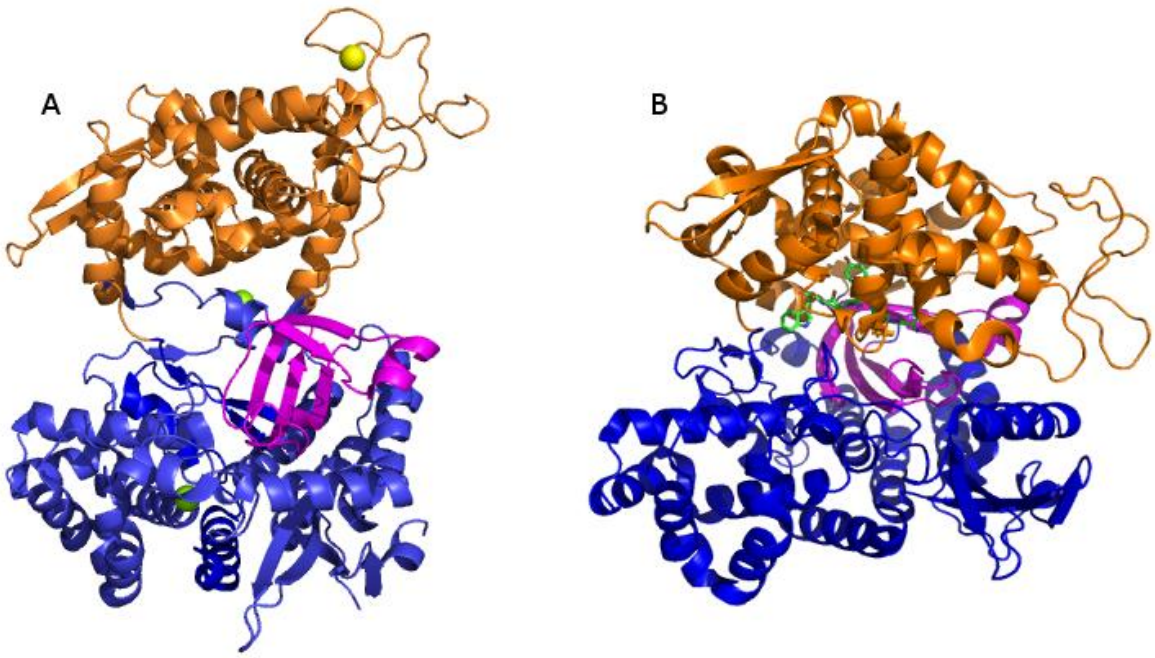

Figure 1: Comparison of open and closed conformation of human DPP III

A: Open unbound conformation of human DPP III. Protein Data Bank Code: 3FVY B: Closed conformation of human DPP III in complex with synthetic hemorphin-like peptide tynorphin (Val-Val-Tyr-Pro-Trp, shown in green) Protein Data Bank Code: 3T6B. Residues contributed from the lower domain of the proteins are coloured in dark blue, residues contributed from the upper domain of the proteins are coloured in orange. The five-stranded β-sheet is shown in magenta. Green spheres: Mg ions, Yellow sphere: Cl ion. Figure created in Pymol.

Proposed catalytic mechanism - In both yDPP III and hDPP III structures, a water molecule has been observed bound to the Zn ion, which completes its tetrahedral coordination. Since this interaction resembles that of other, structurally unrelated metallopeptidases such as thermolysin and neprilysin, the catalytic mechanism of DPP III was proposed to be similar [16,17,18]. In this mechanism, the catalytically essential Glu451 residue, located on the

^{450}HEXXGH^{455} conserved structural motif, acts as a general base and deprotonates the water molecule bound to the zinc ion. This facilitates a nucleophilic attack by the water molecule, which attacks the carbonyl carbon of the scissile peptide bond. In order to observe hDPP III in complex with several of its native substrates, site directed mutagenesis was performed, exchanging the Glu451 residue with an alanine. Since this residue is a critical regulator of enzymatic activity in DPP III, mutating it to alanine renders the enzyme inactive.

Aims of the Thesis - Since only few structures of yDPP III and hDPP III have formerly been solved and characterized, the exact mechanism of substrate binding and catalysis is still largely unclear. This study primarily aims to shed light on the capability of DPP III to adapt to peptide substrates of various lengths and amino acid compositions. Therefore, we purified and co-crystallized inactive hDPP III in complex with several peptide ligands, that were shown to be hydrolyzed by the enzyme in previously performed enzymatic characterization studies [2, 8, 19]. Additionally we purified and crystallized with orthologous DPP III sequences extracted from rat and pig. All constructs used in this study were shortened by 11 amino acid residues from the C-terminus. This region was predicted to be unordered and therefore unfavourable towards crystal formation. Additionally, the shortened constructs differ from the wild type of DPP III (wt DPP III) by the following mutations: C19S, E207C, S491C, C519S, and C654S. These point mutations were originally introduced for single molecule fluorescence resonance energy transfer experiments (sm-FRET). In the inactive variant of hDPP III, the catalytic Glu451 residue present on the HEXXGH motif, is mutated to alanine.

We co-crystallized hDPP III with IVYPW, which is a derivative of the synthetic opioid peptide tynorphin. This compound, with the amino acid sequence of Val-Val-Tyr-Pro-Trp, is the only opioid peptide previously crystallized in complex with human DPP III (Protein Data Bank code: 3T6B) [11]. Furthermore, we also co-crystallized hDPP III with the synthetic ligand (S)-hydroxyethylene (SHE). This ligand was designed in a transition state peptidomimetic approach, with the purpose of inhibiting hydrolytic activity of DPP III in mind.

Additionally, co-crystallization attempts with known in vitro substrates of DPP III were carried out in the same project. These substrates included the endogenous opioid peptides leu-enkephalin, met-enkephalin, valorphin, endomorphin-2 as well as the peptide hormone angiotensin-II. Obtained datasets of hDPP III in complex with angiotensin-II and leu-enkephalin were processed and refined by Prashant Kumar. Datasets of DPP III in complex with met-enkephalin and endomorphin-2 were processed and refined by Viktoria Reithofer. Additionally, since there was no thermodynamic data for the interactions of angiotensin-II with hDPP III available, corresponding ITC measurements were also performed in this study.

Furthermore, we investigated a possible anion- π interaction between the catalytic Glu451 residue and the aromatic ring of Phe373. In this type of interaction, noncovalent forces between electron deficient aromatic systems and anions are utilized to position a residue which can function as a general acid or base, such as glutamic acid or aspartic acid [20]. This interaction might be responsible for correctly positioning the catalytic Glu451 residue in the active site [20,21]. In order to confirm this interaction, an additional construct of active human DPP III was created, which exchanges Phe373 with a leucine residue. This variant will be referred to as F373L DPP III. In the absence of an aromatic ring, this potential anion- π interaction is lost entirely. Fluorescent activity assays were carried out with wild type DPP III (wt DPP III) and the F373L construct using arginine-arginine-β-naphthylamide (Arg_2-βNA) as a substrate [7]. Arg_2-βNA was chosen for this purpose, because it is effectively hydrolyzed by DPP III and the release of the resulting β-naphthylamide (βNA) product can be easily detected. The F373L construct exhibited a 20fold decrease in hydrolytic activity when compared to the wild type enzyme.

2. Materials and methods

2.1 Site-directed mutagenesis and plasmid isolation

DPP III constructs - All experiments performed in this study were carried out using C-terminally shortened versions of DPP III. These variants of rat and, pig as well as human active, inactive and F373L DPP III were created via site directed mutagenesis. The native proteins were shortened by 11 amino acids from their respective C-termini. The genes encoding these truncated versions were cloned into the expression vector pET28-MHL, which is optimized for expression in *Escherichia Coli*. This vector includes an N-terminal His_6-tag sequence, as well as a Tobacco Etch Virus (TEV) protease cleavage site, which were both utilized during protein purification.

The constructs used in crystallization trials were originally created for sm-FRET experiments and deviate from the wild type of human DPP III by the following point mutations: C19S, E207C, S491C, C519S, and C654S. Additionally, one construct of human DPP III also contains the point mutation E451A, which renders the enzyme inactive. Therefore this construct will be referred to as inactive hDPP III. Furthermore, the point mutation F373L was introduced into the sequence of active human DPP III. This F373L mutant was used in fluorescenct activity studies.

Site directed mutagenesis - The primers used in site directed mutagenesis experiments were designed with the QuikChange Primer Design online tool, provided by Agilent Technologies. Said primers are depicted in table 1. Two separate PCR reaction mix solutions were prepared, both with 5 µl of 10 µM primers, 5 µl of 2 mM dNTP's, 1 µl of Phusion polymerase (Thermo Fisher) at 2000 U ml^{-1}, 10 µl of 5x Quick solution (Thermo Fisher) and 100 ng of DNA template, filled up to 50 µl with distilled water. One solution contained only the forward primer and one with the corresponding reverse primer instead. The PCR temperature protocol is depicted in table 2.

Table 1: Forward and Reverse Primer for site-directed mutagenesis of all DPP III variants

Primer Name	Length [nt]	Primer Sequence (5´to 3´)
rat forward	43	Ggtgcttcttgaacctgatcttaccaaaactgtgcatctgcgg
rat reverse	43	Ccgcagatgcacagttttggtaagatcaggttcaagaagcacc
pig forward	35	Gtgcttcacaaggacgttaccaaaagcgtgcatct
pig reverse	35	Agatgcacgcttttggtaacgtccttgtgaagcac
F373L forward	29	Cgtccaggctagtgaggtccggagtcagg
F373L reverse	29	Cctgactccggacctcactagcctggacg

Table 2: Thermocycler program for PCR used in site-directed mutagenesis

Step	Temperature [°C]	Time	No. of Cycles
Initial Denature	95	55 sec.	1
Denature	95	55 sec.	22
Annealing	60 / 58 for F373L	55 sec.	
Extension	72	8 min.	
Final Extension	72	8 min.	1

In order to prevent primer-dimer formation, the PCR reaction was halted temporarily after 4 elongation cycles were completed and 25 µl of the reaction mix containing only forward primer were added to the reverse primer mix and vice versa. The PCR reaction was then restarted and proceeded as described in table 2.

The resulting PCR products were digested by adding 1,5 µl of DpnI protease of 20000 U ml^{-1} and incubating for 2 h in a 37°C water bath. 10 - 50 ng of the DpnI digested amplicons were added to 200 µl of *E. Coli* Top 10 competent cells. Transformation was performed via heat shock treatment for 90 sec at 42°C, followed by 5 min at -4°C. Afterwards, 700 µl of autoclaved lysogeny broth (LB) medium was added and incubated at 37°C for 30 min. After a short centrifugation step, the cell pellets were resuspended and plated on antibiotic selection plates, containing 50 µg ml^{-1} of kanamycin. These plates were incubated over night at 37°C.

Transformation and Plasmid isolation - Liquid over night cultures (ONCs), containing 50 µg ml^{-1} of kanamycin in 10 ml LB medium were prepared, and incubated with resuspended colonies chosen from the aforementioned antibiotic selection plates. These cultures were incubated over night at 37°C. From these ONCs, plasmids were isolated using a MiniPrep kit (Qiagen), according to protocol. The isolated plasmids were analysed by sequencing and plasmids containing the correct sequence were transformed into *E. coli* BL21 Codon Plus expression cells, using the same heat shock treatment method. Stock cells of these transformants were created by adding 350 µl of autoclaved 86% glycerol to 650 µl of ONC, flash cooling with liquid nitrogen and storing them at -80°C.

2.2 Protein expression and purification

Expression- Starter cultures of 10 ml LB medium containing 50 µg ml^{-1} kanamycin antibiotic were prepared and incubated with 3 - 5 µl of stock cells over night at 37°C shaking. Expression cultures of 700 ml LB containing 50 µg ml^{-1} of kanamycin were incubated with 3 ml of the starter cultures and kept at 37°C shaking until OD_{600} reached 0.5 - 0.8. Protein expression was then induced with 0.4 mM isopropyl-1-thio-D-galactopyranoside (IPTG). The induced expression cultures were then kept over night at 18°C shaking. Cells were harvested by pelleting at 6000 rpm with a Sorvall Evolution RC centrifuge, rotor type: SLC 4000 for 20 min at 4°C. Cell pellets were resuspended in 100 mM NaCl, followed by centrifugation at 4000 rpm with the same centrifuge, but rotor type SH 3000 instead, for 40 min at 4°C. The supernatant was discarded, cell wet weight was recorded and the pellets were stored at -80°C for future protein purification.

Purification - Cell pellets were resuspended in buffer, consisting of 300 mM NaCl, 50 mM Tris-HCl, 5 mM imidazole and 1 mM of Tris-(2-carboxyethy) phosphine (TCEP) at pH 8.0. The resuspended pellets were lysed with a probe sonicator. To prepare the sample for purification by chromatography, centrifugation was performed at 18000 rpm with a Sorvall

Evolution RC centrifuge, rotor Type: SA 300 for 60 min at 4°C. The supernatant was filtered, using 0.45 µm pore size syringe filters.

Affinity chromatography was performed on two consecutive GE Healthcare His-Trap Fast Flow columns of 5 ml volume each, packed with nickel-nitrilotriacetic acid (Ni-NTA). The columns were equilibrated with 5 column volumes of an equilibration buffer consisting of 300 mM NaCl, 100 mM Tris-HCl and 1 mM TCEP at pH 8.0.. The protein sample was then applied to the columns and washed out in a gradient elution, using elution buffer consisting of 300 mM NaCl, 100 mM Tris-HCl, 500 mM imidazole and 1mM TCEP at pH 8.0. Protein fractions were collected and their purity was analysed using sodium dodecylsulfate polyacrylamide gel electrophoresis (SDS PAGE), with 12% Tris/glycin. Molecular weight of the protein bands was evaluated using Pierce unstained protein molecular weight marker (Thermo Scientific). All gels were stained with Coomassie Brilliant Blue dye. Suitable protein fractions were unified and their concentration was determined via spectrophotometric measurements using NanoDrop method.

In order to cleave off the His_6-tag sequence, 100 µg of TEV protease per mg of protein were added to the pooled protein fractions and incubated over night. The cleaved DPP III was then dialysed against 50 mM Tris-HCl and 300 mM NaCl at pH 8.0 and 4°C over night. Dialysis was performed using Spectra/Por 4, dialysis tubing, for 12-14 kDa, at a total volume of 2 l. For inactive variant of hDPP III, Zn-ion chelating agents were added, according to table 3, during TEV cleavage and dialysis. After dialysis, another 100 µg of TEV protease per mg of protein were added and incubated at room temperature for 1 h. During the purification of the active hDPP III variant, no zinc ion chelating agents were added in dialysis.

Table 3: Buffer composition of Zn chelating agents, added during dialysis of DPP III

Duration	Buffer composition
3 h	50 mM Tris-HCl pH 8.0, 300 mM NaCl, 4 mM EDTA
3 h	50 mM Tris-HCl pH 8.0, 300 mM NaCl, 4 mM EDTA
3 h	50 mM Tris-HCl pH 8.0, 300 mM NaCl, 4 mM EDTA
3 h	50 mM Tris-HCl pH 8.0, 300 mM NaCl, 30 mM dipicolinic acid
3 h	50 mM Tris-HCl pH 8.0, 300 mM NaCl, 30 mM dipicolinic acid
3 h	50 mM Tris-HCl pH 8.0, 300 mM NaCl
Overnight	50 mM Tris-HCl pH 8.0, 300 mM NaCl
2 h	50 mM Tris-HCl pH 8.0, 300 mM NaCl

Reverse affinity chromatography was performed on one GE Healthcare His-Trap Fast Flow column of 5 ml volume. The equilibration buffer consisted of 50 mM Tris-HCl pH 8, 300 mM NaCl and 1 mM TCEP and the elution buffer contained 50 mM Tris-HCl pH 8, 300 mM NaCl and 500 mM imidazole. The column was equilibrated using 5 column volumes of equilibration buffer. After gradient elution, using an increasing concentration of imidazole, protein fractions were collected at a fraction size of 4 ml and analysed via 12% Tris/glycin SDS PAGE, as described before.

Usable protein fractions were pooled and used in an anion exchange chromatography, performed with a prepacked ResourceQ GE Healthcare column of 6 ml volume. Collected protein fractions were diluted with anion exchange equilibration buffer, consisting of 20 mM Tris - HCl at pH8, in order to reduce salt concentration down to 100 - 150 mM. The column was equilibrated with 5 column volumes of equilibration buffer and the protein sample was applied to the column. Protein fractions were collected in a gradient elution using an increasing NaCl concentration, up to 1 M. Fractions were collected at 0,5 ml volume and their purity was again analysed with a 12% Tris/glycin SDS PAGE.

Lastly, size exclusion chromatography was performed, using a Superdex 200 26/60 GE Healthcare gel filtration column. The column was equilibrated, using a multicomponent buffer, consisting of 1 mM TCEP, 150 mM NaCl, 100 mM Tris-HCl, 100 mM Mes, 100 mM Malic acid at pH 8.0 [22]. For protein collection, a fraction size of 2 ml was chosen. Purity of the collected fractions was analysed by 12% Tris/glycin SDS PAGE. Suitably pure fractions were pooled and concentrated with via centrifugation at 4000 rpm (Eppendorf 5810R centrifuge), using a centricon tube with a pore size of 30 kDa. These purified, concentrated proteins were then immediately used in crystallization trials.

2.3 Crystallization

The purified protein was centrifuged for 15 min at 14000 rpm in an Eppendorf 5810R centrifuge, in order to dispose of precipitation. All crystallization experiments were performed, using a sitting drop vapor diffusion setup. 96-well SwissSci Triple Drop plates (Molecular Dimensions) were used and all screening plates were kept at 20°C. Proteins utilized in these crystallization trials were used immediately after purification, without flash cooling them beforehand.

Primary screening - The initial screening experiments were carried out, using the Hampton Research primary crystallization screens Index, JCSG, Crystal, Salt RX, Morpheus, PEG/Ion and Midas. Further optimizations of the conditions, as well as microseeding experiments to improve crystallization results and crystal quality were also performed. All crystallization approaches were carried out, with both protein and ligand dissolved in 100 mM of multicomponent buffer, which also contained 150 mM of NaCl, in order to be consistent with the last step of protein purification.

Co-crystallization - All co-crystallization trials used 0.056 M sodium phosphate monobasic monohydrate, 1.344 M potassium phosphate dibasic at pH8.2 as their reservoir condition (Index Screen Condition #19, Hampton Research). This condition was also used to obtain the first structure of the inactive DPP III variant in complex with the synthetic peptide ligand tynorphin [11]. A total

drop volume of 1.2 µl was chosen, with initial screening experiments performed with 0.6 µl of protein and ligand, as well as 0.6 µl of reservoir condition. While later microseeding experiments were performed with 0.6 µl of protein and ligand, 0.4 µl of reservoir condition and 0.2 µl of microseeds.

In order to co-crystallize human DPP III with various peptide ligands, the protein was concentrated to 8, 10 and 12 mg ml^{-1} and protein-ligand ratios of 1+5, 1+10 and 1+30 were used for for endomorphin-II. Met-enkephalin and leu-enkephalin were co-crystallized at 1+10, 1+20 and 1+30 and crystallization trials with valorphin were conducted with a protein-ligand ratio of 1+50. SHE was co-crystallized at 1+1, 1+2 and 1+3 protein-ligand-ratio and IVYPW was co-crystallized at ratios of 1+0.5, 1+1 and 1+20.

Microseeding - Seeding stock for microseeding experiments was produced, using insufficiently formed crystals from primary screening experiments with inactive hDPP III in complex with angiotensin-II. The crystals in question were crushed with a probe, then transferred to test tubes containing a seed bead in 50 µl of Index screen condition #19 (Hampton Research). The test tubes were vortexed for 2 min, stopping every 30 sec to cool the test tube on ice. The resulting seed stocks were frozen in liquid nitrogen and kept on -80°C.

Optimization - After initial promising results from rat and pig DPP III crystallization attempts on PEG/ion screens, additional optimization experiments were carried out. These experiments used 0.2 M $MgSO_4$ heptahydrate and 20% w/v polyethylene glycol (PEG) 3350 (PEG/Ion screen condition #32, Hampton Research) as their reservoir condition. Concentration of $MgSO_4$ was varied between 0.05 and 0.035M and PEG concentration was varied between 5% and 30%. Protein concentrations of 9, 12, and 15 mg ml^{-1} were used in these optimization attempts, with and without cross seeding. Cross seeding was carried out, using seeds produced from crystals of inactive human DPP III in complex with angiotensin-II, which was produced in the same project as described above.

Crystals were kept at 20°C for one month, then subsequently stored for data collection, by flash cooling to -173.15°C in liquid nitrogen, without applying any additional cryoprotectants.

2.4 Data collection and structure determination

Diffraction data sets, used in solving crystal structures were collected at beamline ID29 (Grenoble, France). Initial data reduction and processing was performed with XDS software [23]. In order to solve the structure, the molecular replacement method was carried out in the program PHASER from the CCP4i program suite (Collaborative Computational Project, Number 4, 1994), using the tynorphin bound, hDPP III structure (Protein Data Bank code: 3T6B, *Bezerra et al*., 2012) as a search model [24]. Further iterative refinement steps were performed in PHENIX software [25]. The program COOT was used for model fitting and real space refinement, using σA-weighted 2Fo-Fc and Fo-Fc electron density maps [26]. Stereochemistry of the refined crystal structures was checked and validated with the Molprobity online tool.

2.5 Fluorescent activity assay

The enzymatic activities of the purified DPP III variants F373L and wt DPP III were determined in a spectrophotometric activity assay, similar to the assays descirbed by *Jajčanin-Jozić et al* in [7]. Protein concentration for wt DPP III of 20 pM was chosen, while F373L was measured at 500 pM, since the activity of this DPP III variant was predicted to be lower. All proteins stocks were prepared in buffer containing 50 ml Tris-HCl and 150 ml NaCl at pH 8. The substrate, Arg-Arg-2-naphthylamide (Arg_2-βNA) was prepared in 50 mM Tris-HCl, 100 mM NaCl buffer at pH 8.0. Several different substrate concentrations were prepared, ranging from 0.5 μM up to 500 μM and measured for 5 minutes each. All experiments were performed at 37°C and the detector slit width was set to 4 μm. During the course of the reaction, the two arginine residues of the substrate are cleaved off in hydrolysis, leaving the fluorogenic ß-naphthylamine (ß-NA) product, which can be detected. An excitation wavelength of 340 nm and an emission wavelength of 420 nm were used to detect increasing concentrations of the catalytic reaction product ß-NA, during the course of the assay.

In order to create a calibration curve, the fluorescence activity of ß-NA was measured for substrate concentrations ranging from 0.01 µM up to 2 µM. This calibration curve relates the absorbance of ß-NA to product concentration. Data analysis and calculation of enzymatic activity were performed using GraphPadPrism 5 software in order to calculate enzyme velocity in pM s^{-1}, michaelis menten constant K_M, turnover number K_{cat} and maximum reaction velocity V_{max}.

2.6 Isothermal titration calorimetry

In order to obtain thermodynamic data for the interaction between the bioactive peptide angiotensin-II and hDPP III, ITC experiments were carried out in this study. The E451A variant of hDPP III was chosen for this purpose, because it is inactive and therefore binds to angiotensin-II without processing it. The ligand was dissolved in buffer containing 50 mM Tris-HCl and 100 mM NaCl at pH 8.0. Measurements were taken with a VP-ITC calorimeter (MicroCal, Northampton) equilibrated at 25°C. Protein concentration was set to 40 µM and ligand was prepared in 800 µM concentration. Both ligand and protein were degassed immediately before measurements were taken.

The titration experiment consisted of 30 injections, one aliquot of 2 µl peptide solution, followed by 29 aliquots of 10 µl peptide solution. The peptide was injected at a rate of 0.5 µl sec^{-1}, over 20 sec. into 1.421 ml of protein solution under constant stirring at 270 rpm. Spacing time between injections was set to 225 sec. As a blank measurement, 800 µM of peptide solution was injected into buffer only, in the same manner as described above. The results of these blank measurements were subtracted from the measurement data.

Data analysis was performed with Origin software (Version 7.0, MicroCal) using the non linear least square fitting method to calculate reaction stochiometry (n), enthalpy (ΔH), entropy (ΔS) and binding constant (K_D). Furthermore, the Gibbs-Helmholtz equation was used in order to calculate changes in Gibbs energy (G) of the system, as a function of temperature.

3. Results

3.1 Protein purification

Protein expression was performed overnight at 18°C. Cells were harvested, washed and pelleted. The received cell pellets were lysed, using sonication. The resulting cell extract was filtered with syringe pore filters and loaded on a (Ni-NTA) packed His-Trap column for affinity chromatography. Afterwards, a Coomassie stained SDS-PAGE was performed, in order to find fractions with a high amount of protein. As can be seen in figure 2, a strong band between 66.2 kDa and 116 kDa indicates a high rate of expression for hDPP III, which should appear at approximately 82 kDa. Additional steps were taken in order to cleave of the N-terminally bound His_6-Tag sequence and to separate hDPP III from impurities present in these fractions.

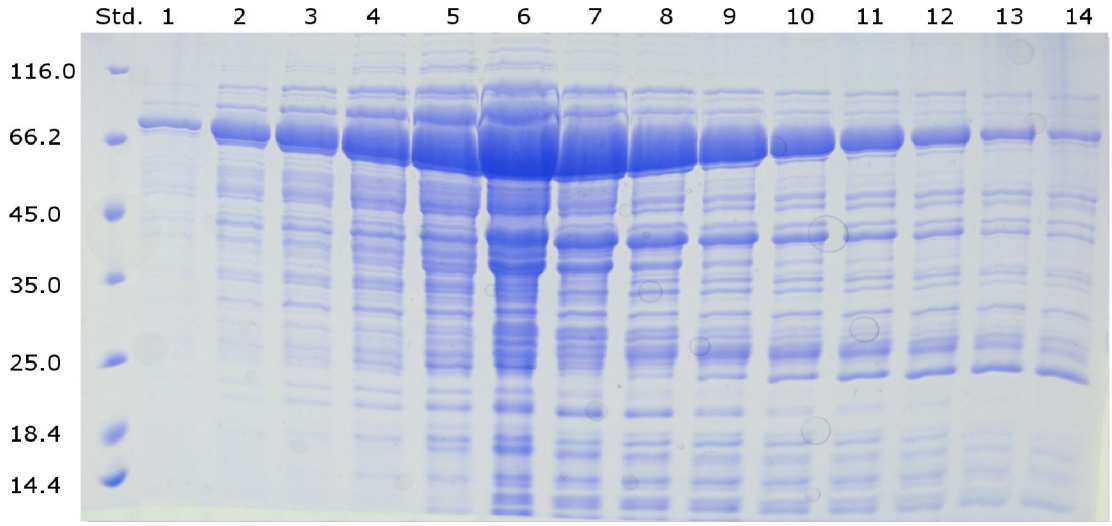

Figure 2: SDS-PAGE after affinity chromatography of inactive hDPP III.

Std: Unstained protein molecular weight marker; Bands 1 - 14 contain filtrated and lysed cell extract. The band for DPP III can be seen at 82 kDa. The gel was stained with Coomassie brilliant Blue.

After collecting and pooling fractions with a high amount of protein, overnight dialysis was performed while simultaneously removing the N-terminal His_6-Tag,

by cleaving it with TEV protease. Reverse affinity chromatography was then performed to separate the properly cleaved protein from the His_6-Tag and from protein fractions that were not properly cleaved by the TEV protease. Figure 3 shows the SDS-PAGE after performing reverse affinity chromatography. The upper strong band contains the protein, while the lower, weaker bands observable in most fractions consists most likely of degradation products of DPP III. Since these degradation products would reduce the quality of the desired protein crystals, further purification steps were deemed to be necessary.

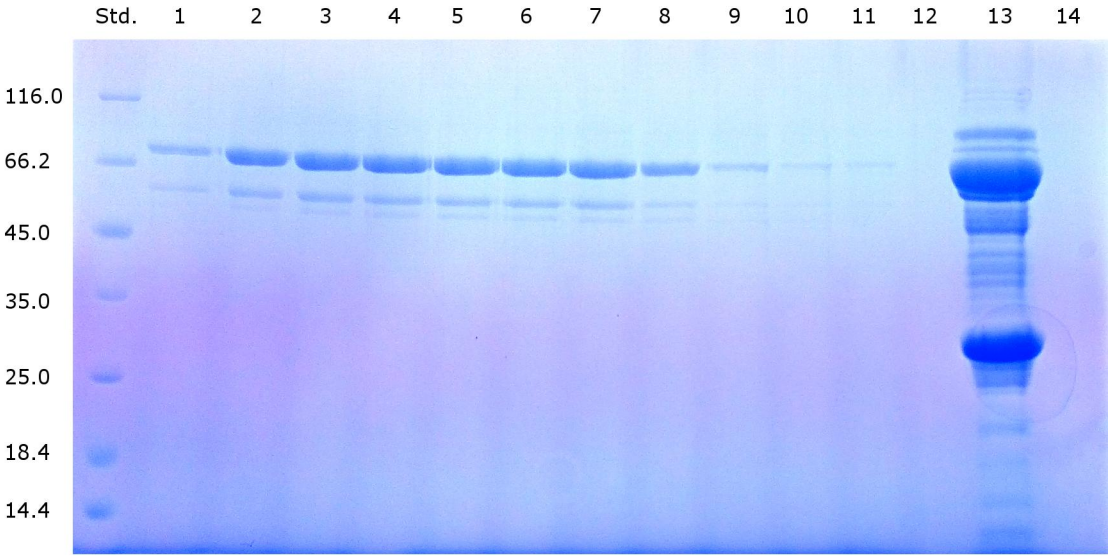

Figure 3: SDS-PAGE after reverse affinity chromatography of inactive hDPP III

Std: Unstained protein molecular weight marker; Bands 1 - 12 contain pooled fractions of hDPP III after dialysis and TEV digestion; Band 13 contains TEV protease and hDPPII with His_6 Tag still attached. The gel was stained with Coomassie brilliant Blue.

Anion exchange chromatography was performed in order to separate proteins of different charges. The weaker bands below DPP III, present in figure 4 indicate, that there are still impurities from unspecifically bound proteins present in the pooled fractions.

As a final step of purification, size exclusion chromatography was used to separate proteins of different sizes and molecular weights. The resulting

protein fractions, as depicted in figure 5 were pooled, concentrated and then used in crystallization trials immediately afterwards.

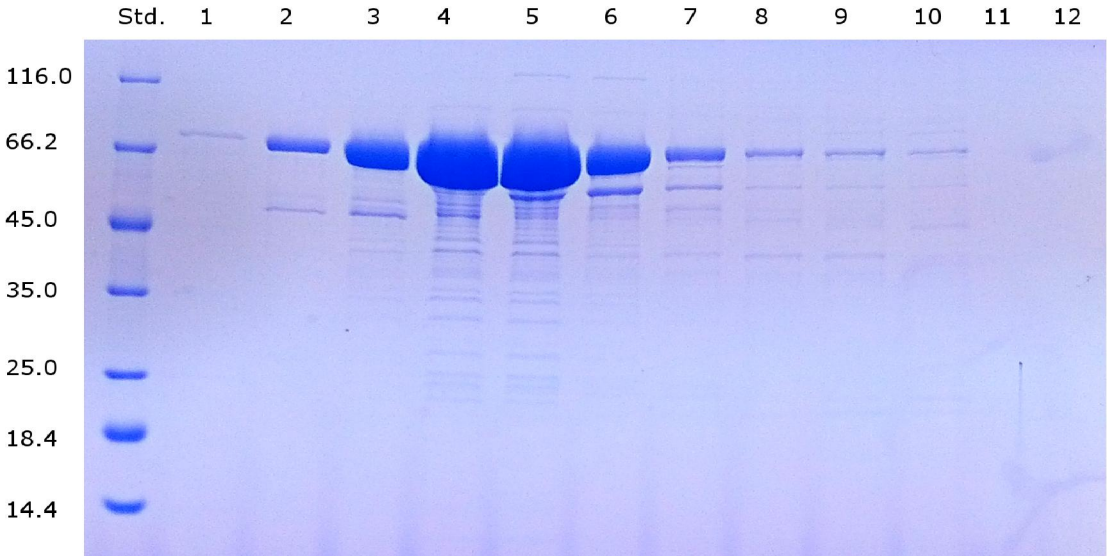

Figure 4: SDS-PAGE after anion exchange chromatography of inactive hDPP III

Std: Unstained protein molecular weight marker; Bands 1-12 contain fractions of collected hDPP III. All fractions were stained with Coomassie brilliant Blue.

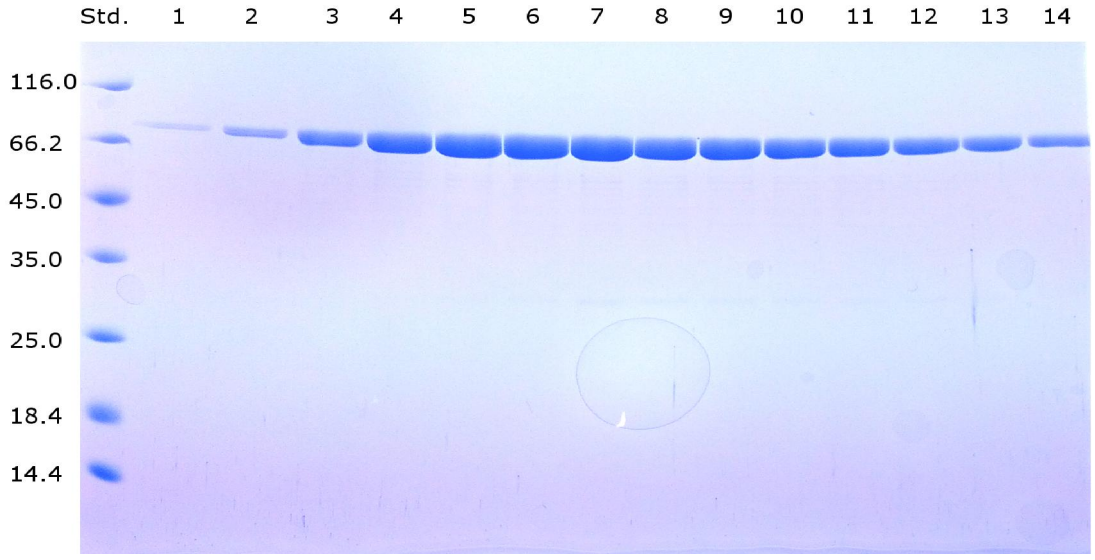

Figure 5: SDS-PAGE after size exclusion chromatography of inactive hDPP III

Std: Unstained protein molecular weight marker; Bands 1-14 contain fractions of collected hDPP III. The gel was stained with Coomassie brilliant Blue.

3.2 Crystal structures

In this work, we present crystal structures obtained from the inactive hDPP III variant in complex with the synthetic ligands SHE and IVYPW, designed to inhibit DPP III enzymatic activity. Substrate bound structures, which were also obtained in the same project, will be described and discussed in more detail in the following chapter. The active variant of DPP III, as well as orthologous DPP III sequences from rat and pig, unfortunately did not yield diffraction quality crystals. All structures were obtained in co-crystallization trials using a sitting drop vapor diffusion setup, incubating for at least one week in a 20°C environment. The first structure to be successfully determined was hDPP III in complex with angiotensin-II. In this case, the drop size was set to 1.2 µl, with 0,6 µl of Index condition #19 and 0,6 µl of protein and ligand in multicomponent buffer. The protein was concentrated to 8 mg ml^{-1} and the protein-ligand ratio was 1+30. This crystallization trial yielded poorly formed crystals, which were used as seeding stock in the following microseeding experiments.

In further co-crystallization trials, microseeding was performed with seeding stock obtained from the angiotensin-II experiment, which led to diffraction quality crystals appearing significantly faster. The remaining crystals were obtained within a week, as opposed to several months. For these experiments, the drop size was again set to 1.2 µl with 0,6 µl of protein and ligand in mutlicomponent buffer, 0.4 µl of Index screen condition #19 and 0.2 µl of seeding stock. The protein crystals which yielded diffraction data sets were received at protein-ligand ratios of 1+30 for met-enkephalin, leu-enkephalin and endomorphin-2, 1+5 for SHE and 1+3 for IVYPW. All protein crystals were obtained with freshly purified protein, which was not flash frozen in liquid nitrogen before use.

X-Ray diffraction revealed, that all structures received in this project crystallized in the monoclinic C2 space group with one molecule per asymmetric unit. Crystal parameters and refinement statistics for IVYPW - and SHE bound hDPP III are described in detail in table 4. All crystals chosen for X-Ray diffraction measurements displayed the same morphology. An example

can be seen in figure 6. Of all determined crystal structures, met-enkephalin bound DPP III yielded the highest resolution at 1.8 Å. Since all six structures were found to be isomorphous, the met-enkephalin bound structure was used as a refinement model, in order to facilitate structure determination of the other crystal structures.

Figure 6: Crystal morphology of inactive hDPP III in complex with leu-enkephalin

Picture taken from hDPP III in complex with leu-enkephalin. Protein in 10 mg ml^{-1} concentration, with protein-ligand ratio of 1+30. Reservoir condition was 0.056 M sodium phosphate monobasic monohydrate, 1.344 M potassium phosphate dibasic, pH 8.2

Table 4: Crystal parameters and refinement statistics of hDPP III in complex with synthetic ligands IVYPW and SHE. Values in parentheses represent the highest resolution shell.

	hDPP III + IVYPW	**hDPP III + SHE**
Crystal Parameters		
Program	XDS	XDS
Synchrotron	ESRF ID29	ESRF ID29
Space Group	C 1 2 1	C 1 2 1
Unit Cell parameters [Å,°]	1119.55, 105.75, 64.99, 90, 93.43, 90	119.337, 105.587, 64.861, 90, 93.65, 90
Data Collection		
Resolution [Å]	45.56-2.76 (2.86-2.76)	45.28-2.646 (2.74-2.646)
Wavelength [Å]	0.972	0.972
R_{merge} [%]	0.211 (0.501)	0.1165 (0.7063)
R_{meas} [%]	0.2466	0.139
$<I/\delta(I)>$	4.39 (0.11)	8.03 (1.54)
R_{pim}	0.122 (0.272)	0.077 (0.42)
Total number of reflections	78751 (6542)	77119 (6908)
No. of unique reflections	20651 (1778)	23081 (2153)
Multiplicity	3.8 (3.7)	3.3 (3.2)
Completeness [%]	97.92 (84.87)	98.29 (92.82)
Wilson B factor	57.44	53.70
$CC_{1/2}$	0.926 (0.734)	0.993
CC*	0.981 (0.92)	0.998
Refinement		
R_{work} [%]	0.20	0.2151
R_{free} [%]	0.25	0.26
Bond lengths [Å]	0.004	0.002
Bond angles [°]	0.58	0.55
Clash score	3.83	3.68
No. Of non-hydrogen atoms	5835	5869
Ligands	4	4
Protein residues	726	726
No. Of water molecules	31	71
Average B factor [$Å^2$]	56.9	48.70
Macromolecule	56.30	48.80
Ligands	53.20	51.40
Solvent	45.40	37.90
Ramachandran analysis		
Favored [%]	97	97
Allowed [%]	2.86	3
Disallowed [%]	0.14	0

3. 2. 1 hDPP III in complex with IVYPW

IVYPW is a synthetic hemorphin analogue pentapeptide, whose skeletal structure is depicted in figure 7. It exhibits a very similar amino acid composition to tynorphin (Val-Val-Tyr-Pro-Trp), with an isoleucine residue instead of valine at the N-terminus being the only difference. Tynorphin is the peptide IVYPW was derived from and the first ligand molecule to be successfully crystallized in complex with human DPP III [10, 14]. Although both valine and isoleucine are aliphatic amino acids of similar size, enzyme inhibition studies performed using several hemorphin-like pentapeptides have revealed IVYPW to inhibit rat DPP III 17.3 fold stronger when compared to tynorphin [19].

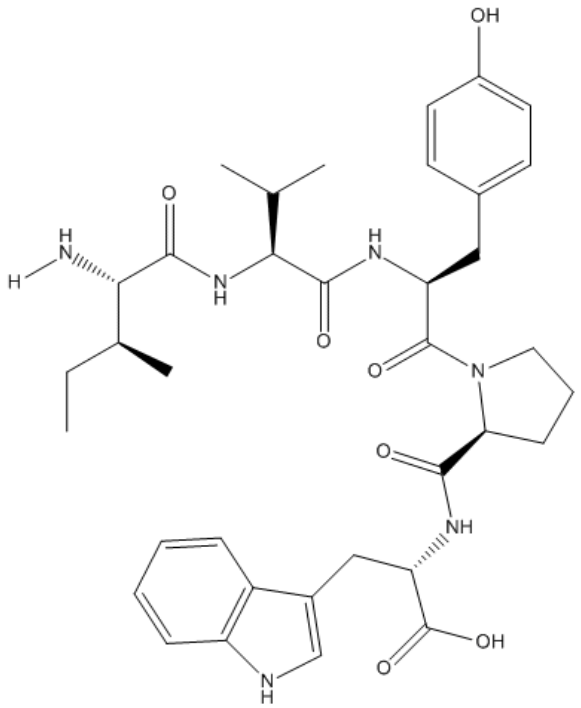

Figure 7: Skeletal formula of IVYPW

Synthetic peptide derived from tynorphin, with strong inhibitory function towards DPP III. Figure created in Chemdraw.

Furthermore, this is the first structure of DPP III in complex with an inhibitor peptide, where the catalytic zinc ion can be observed in the active site. The overall structure, as depicted in figure 8, exhibits a closed conformation with

the inhibitor molecule completely buried in the binding site. The ligand molecule is noncovalently bound to the five stranded β-sheet region on the proteins lower domain, in an antiparallel fashion, which is a common strategy in order to optimize backbone interactions through hydrogen bonds [27]. Most of these noncovalent binding interactions are also contributed by conserved residues from the lower domain of the protein. A potassium ion and two magnesium ions can be observed in this structure as well.

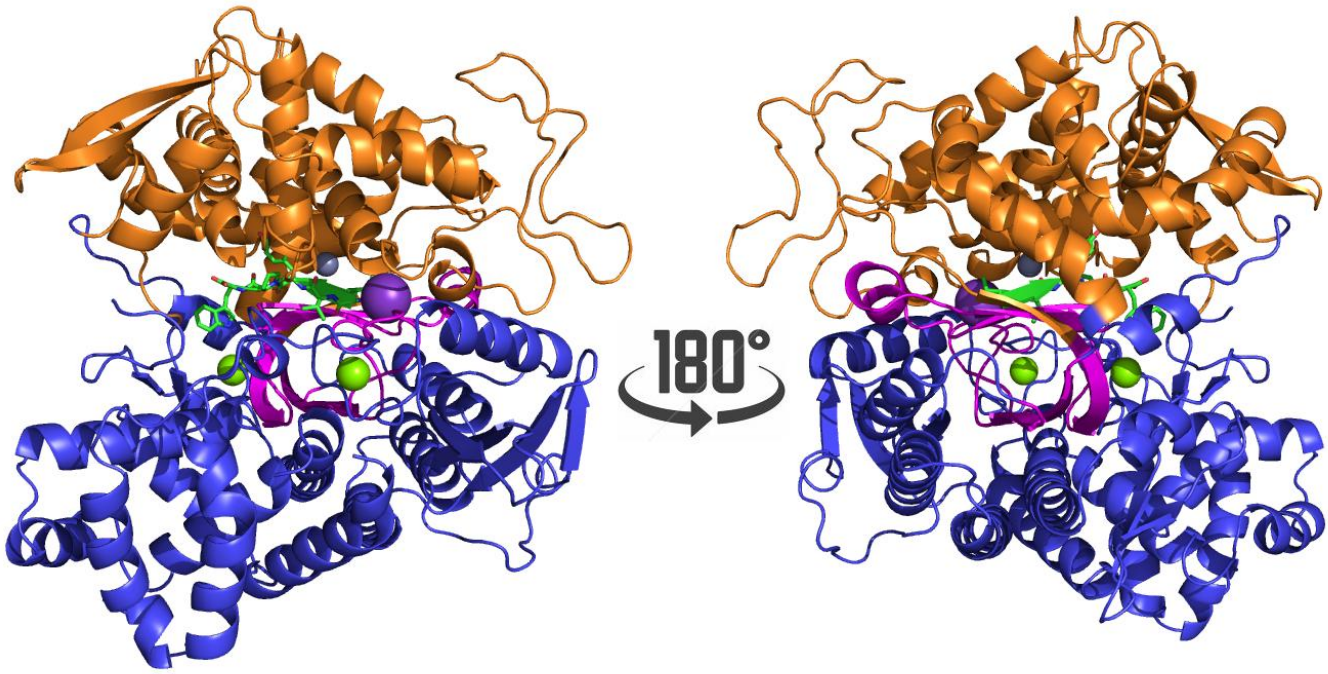

Figure 8: Overall structure of hDPP III in complex with IVYPW

Two perspectives on the overall structure of hDPP III in complex with IVYPW, rotated by 180°. The ligand molecule is shown in green. Upper domain residues are coloured in orange, lower domain residues are coloured in dark blue; The five-stranded β-sheet region is highlighted in magenta. The violet sphere represents a potassium ion; the two green spheres are magnesium ions.The grey sphere is the catalytic zinc ion. Figure drawn in Pymol.

Figure 9 provides a closer look of the inhibitor molecule and its arrangement in the enzymes active site. In this structure, the zinc ion can be observed in contact with the ligand molecule, at the carbonyl end of the proteolytic cleavage site (Val2 residue). A series of hydrogen bonds, contributed from the conserved residues Ala388 up to Asn391 serves to stabilize the inhibitor molecule in its present extended formation. These residues are part of the five stranded β-core region. His568 is the only residue on the upper domain of DPP III interacting with the inhibitor, via a hydrogen bond to the carbonyl carbon of the inhibitors Val2 residue. Furthermore, Arg669 is hydrogen bonded to the C-terminal phenylalanine of the ligand molecule. The conserved residues Asn394, and Tyr318 exhibit electrostatic interactions and hydrogen bonds, which serve to stabilize the N-terminus of the inhibitor in the active site.

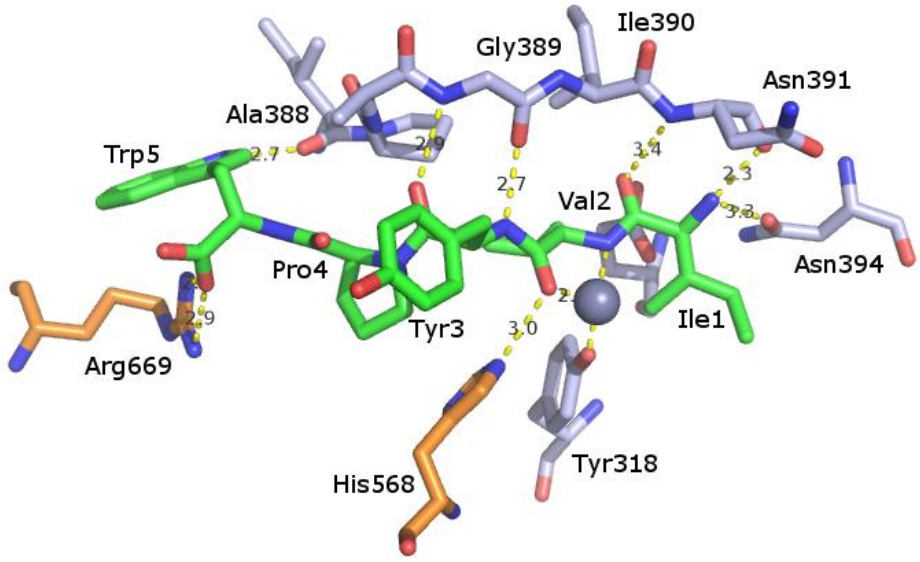

Figure 9: IVYPW bound to hDPPII active site

Active Site residues involved in peptide binding and coordination of the zinc ion. The inhibitor molecule is shown in green. Residues contributed from the lower domain of the protein are coloured light blue, residues contributed from the upper domain are coloured in orange. The grey sphere represents the catalytic zinc ion, scaled to 50% radius. The dashed yellow lines show interaction distances in Å. Figure drawn in Pymol.

Due to these extensive interactions, the electron density map of the ligand molecule appears to be well defined at the N-terminus, as depicted in figure 10. This trend was observed throughout all enzyme-ligand complexes obtained and analysed in this project. The structure of hDPP III in complex with IVYPW has been added to the RCSB Protein Data Bank and can be accessed with the code: 5E3C.

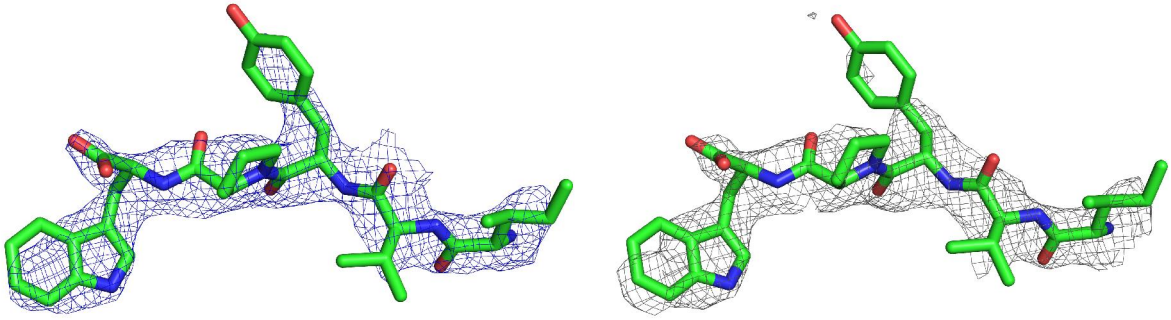

Figure 10: Electron density maps for the IVYPW ligand molecule

Electron density for 2Fo-Fc composite map on the left is contoured at 1.0 δ; The Fo-Fc difference map on the right is contoured at 2.5 δ. This figure was reused from [28]

3. 2. 2 hDPP III in complex with SHE

The synthetic inhibitor (S)-hydroxyethylene (SHE), was designed in a peptidomimetic approach, based on the structure of DPP III in complex with tynorphin [11]. SHE was provided to us by Jakov Ivkovic from the Institute of Organic Chemistry at the Graz University of Technology. (S)-Hydroxyethylene was chosen for this approach, because it is a transition state analogue in the hydrolytic process. Transition state analogues inhibit catalytic reactions by blocking the active site, without getting processed by the enzyme. In the case of SHE, the enzyme is presented with a carbon-carbon bond instead of a peptide bond at the peptide cleavage site, as the skeletal formula depicted in figure 11 illustrates. This carbon-carbon bond exerts a higher bond-dissociation energy and is therefore not as readily hydrolyzed as a peptide bond. Furthermore, because these inhibitors are specifically designed to mimic

the transition state of a reactions, it has been suggested that they form a stronger bond to the enzyme then its actual, native substrates [34].

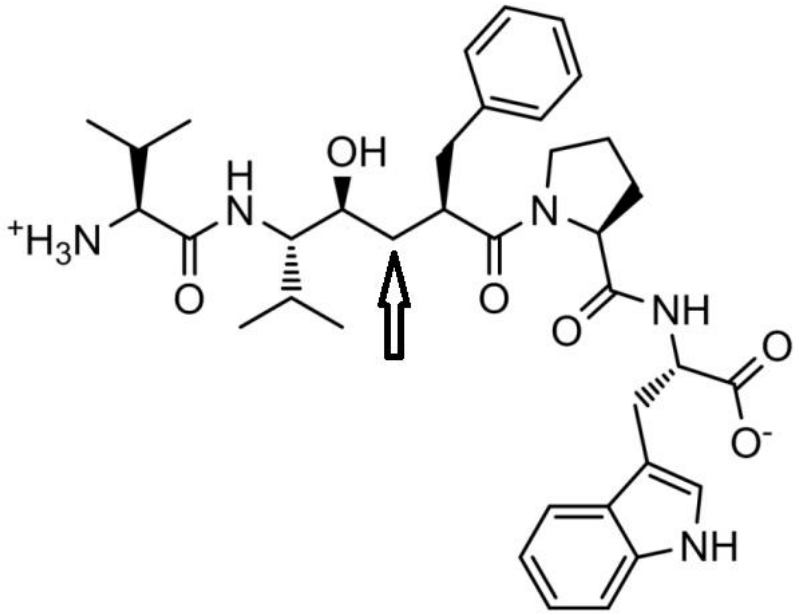

Figure 11: Skeletal formula of synthetic inhibitor (S)-hydroxyethylene

Structure of the synthetic inhibitor peptide S-hydroxyethylene. The arrow points to a C-C bond between C3 and C4, where DPP III would normally facilitate hydrolysis of a peptide bond. This figure was created in Chemdraw.

The overall structure of hDPP III in complex with SHE shows no significant deviations from the others structures we analysed in this project. As figure 12 depicts, the complex is present in its closed conformation, with the inhibitor molecule in the active site. Potassium and magnesium ions, can also be observed in this structure.

Diverging from the other structures however, the SHE molecule appears to interact exclusively with the lower domain of the protein. This can be seen in figure 13, which depicts a close-up of the ligand molecule in the active site. No interaction between the conserved His568 residue and inhibitor could be detected in this instance.

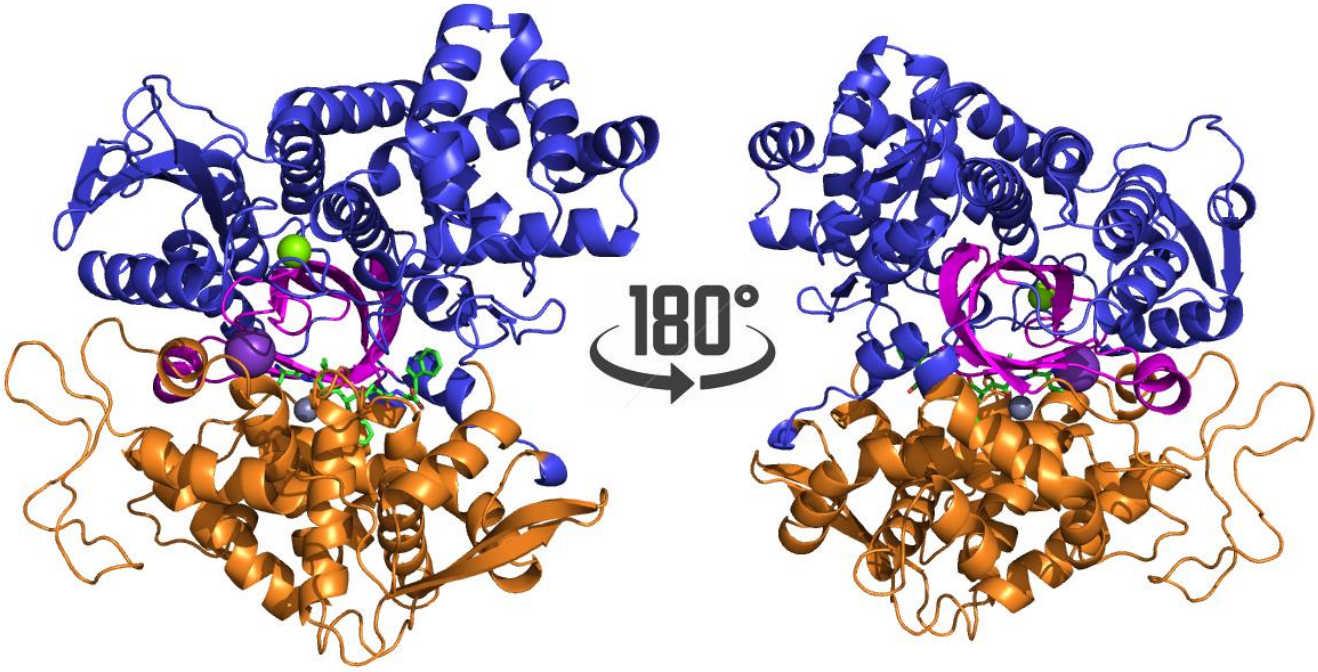

Figure 12: Overall structure of hDPP III in complex with SHE

Two perspectives on the overall structure of hDPP III in complex with SHE, rotated by 180°. The ligand molecule is shown in green. Residues contributed from the upper domain of the protein are coloured in orange, lower domain residues are coloured in dark blue. The five-stranded β-core is highlighted in magenta. The violet sphere represents a potassium ion, the two green spheres are magnesium ions and the grey sphere represents the catalytic zinc ion. This figure was drawn in Pymol.

The catalytic zinc ion is in close proximity to the C4 carbon of hydroxyethylene. As observed in the IVYPW bound structure, the residues from Ala388 to Asn391 form a network of hydrogen bonds with the inhibitor molecule, stabilizing it in its extended conformation. Furthermore, polar interactions contributed from Glu316, Asn391 and Asn394 serve to stabilize the inhibitors N-terminal positioning.

The electron density map for the ligand molecule is depicted in figure 14. Although the electron densities backbone definition is arguably less than ideal, it provides us with sufficient information to place the inhibitor in the active site with reasonable certainty.

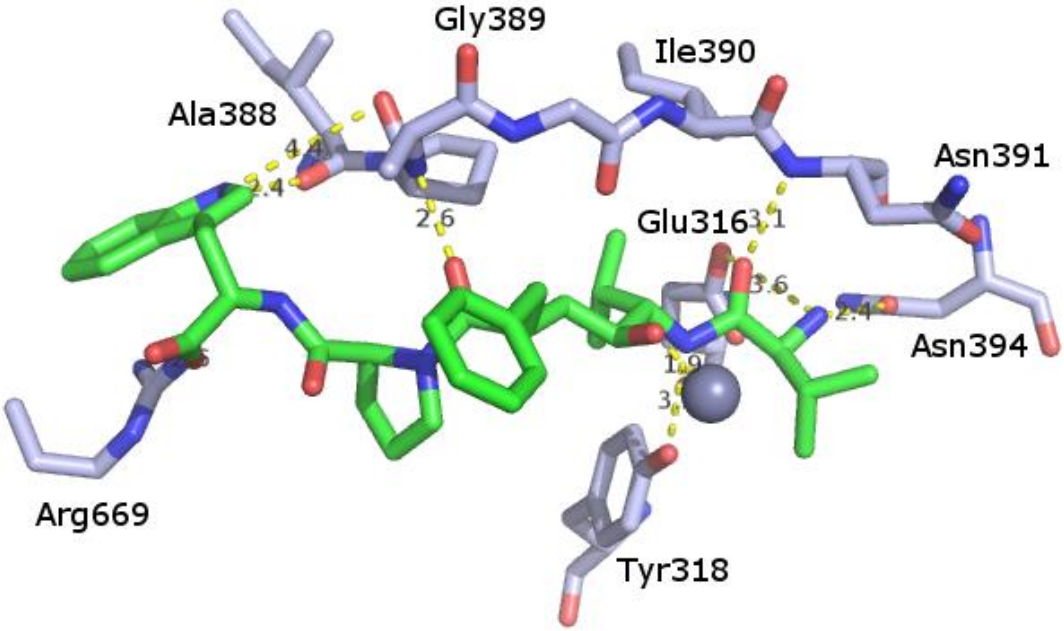

Figure 13: SHE bound to hDPPII active site

Active Site residues involved in peptide binding and coordination of the zinc ion. The inhibitor is shown in green. Residues contributed for the lower domain of the protein are depicted in light blue. The grey sphere represents the zinc ion, sclaed to 50% radius. The dashed yellow lines represent interaction distances in Å. Figure drawn in Pymol.

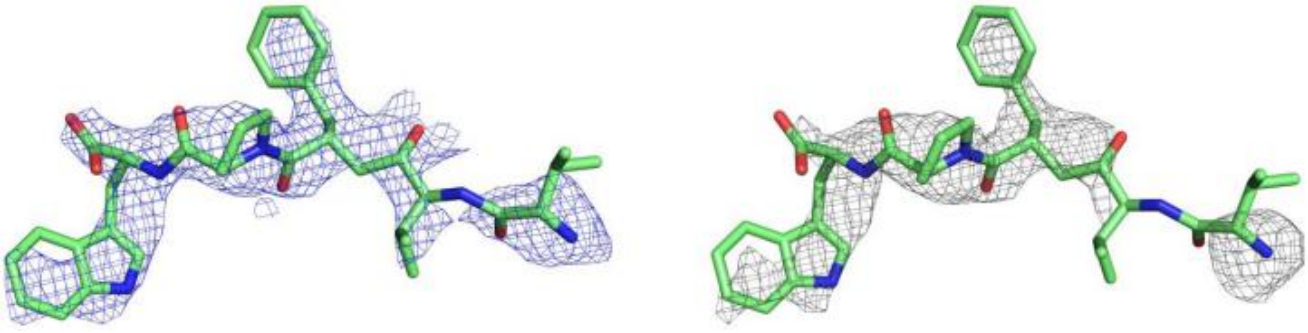

Figure 14: Electron density maps for the SHE ligand molecule

Electron density for 2Fo-Fc composite map on the left is contoured at 1.0 δ; The Fo-Fc difference map on the right is contoured at 2.5 δ. Figure reused from [28]

3.3 Fluorescent activity assay

As suggested by *Schwans et al.*, anion-aromatic interactions might play a significant role in correctly positioning general acids or bases like glutamic acid or aspartic acid in an enzymes active site [20]. These interactions can be utilized in lieu of, or in addition to a network of hydrogen bonds. *Schwans et al.* further emphasized the importance of conserved phenylalanine residues, due to their capability of binding hydrophobic substrates as well [20]. The absence of these stabilizing interactions should display a significant impact on the catalytic activity of hDPP III. In order to verify the importance of this interaction, fluorescence activity assays were performed using a new variant of active hDPP III, with a single point mutation at the conserved Phe373 residue.

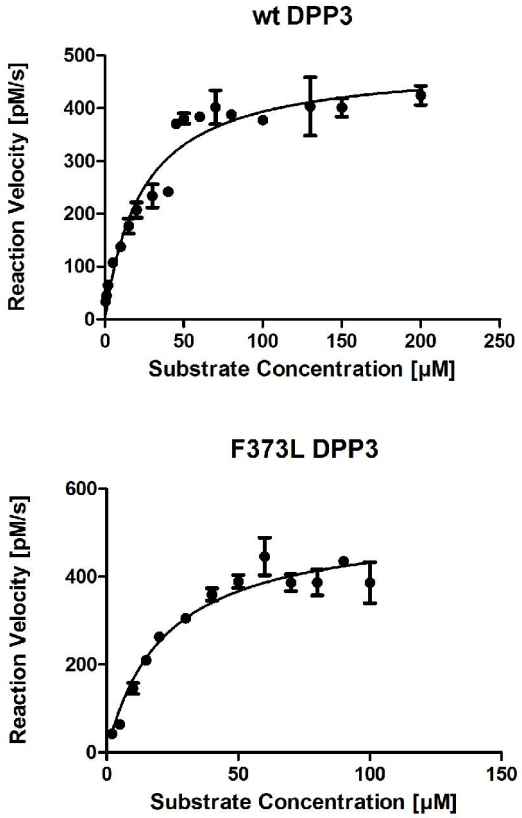

Figure 15: Fluorescent activity assays with wt DPP III and F373L DPP III

Michaelis menten kinetics for both DPP III variants employed in fluorescent activity assays. Top: wt DPP III; Bottom: F373L DPP III. Figure created using Graphpad Prism 5 software.

The top half of figure 15 depicts the michaelis menten kinetics of wild type hDPP III regarding hydrolysis of the Arg_2 -βNA substrate, which results in rising concentration of the product βNA. βNA can be fluorometrically detected at an emission wavelength of 420 nm. Michaelis menten kinetics of the F373L mutant is depicted in the bottom half of figure 15. When comparing the kinetic parameters, shown in table 5, it is important to note that wt DPP III was measured at significantly lower protein concentration. We observed that altough K_M between both reactions remains relatively unchanged, K_{Cat} of the F373L mutant is decreased 24 fold.

Table 5: Comparison of michaelis menten kinetics parameters for both wt DPP III and F373L DPP III variants, used in fluorescent activity assays

Protein	Concentration [pM]	v_{max} [pM s^{-1}]	K_m [µM]	K_{cat} [s^{-1}]
wt hDPP III	20	486.13	23.55 ± 3.53	24.31
F373L hDPP III	500	526.17	21.69 ± 3.63	1.052

3.4 Isothermal titration calorimetry

Besides confirming direct interactions between small molecules and macromolecules, thermodynamic measurements gained from ITC experiments can also help in determining their binding affinity and stochiometry. Because no thermodynamic data for the binding of angiotensin-II to inactive hDPP III have previously been reported, ITC experiments were performed in this study. To this end, a protein concentration of 40 µM and an angiotensin-II concentration of 800 µM was used and heat of dilution was corrected by subtracting data gained in reference measurements. Received data was analysed using Origin software (version 7.0 MicroCal).

The top left half of figure 16 depicts the time course of the experiment, with each peak corresponding to one injection. The bottom left half of shows the peak integral of these injections as a function of hDPPII molar ratio. In the same figure, the table on the right hand side shows the thermodynamic

parameters, calculated from these measurements. For a spontaneous process, the free energy (ΔG) at constant pressure, must be negative, and hence the entropy term has to outweigh the enthalpy term. Therefore, angiotensin-II was found to exhibit an endothermic binding behaviour. This is consistent with the binding mode of other ligands analysed in this study, as well as previous experiments performed with yeast DPP III [11]. The dissociation constant was calculated at 1.64 µM, which suggest a relatively strong binding of the ligand to the enzymes active site.

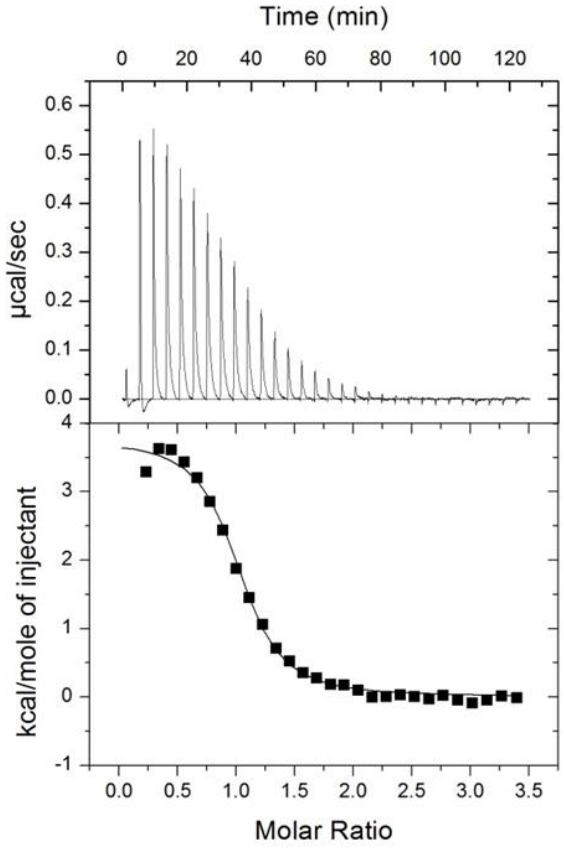

Thermodynamic parameters	Values
K_d [µM]	1.64 ± 0.12
ΔH [kJ.mol^{-1}]	15.25 ± 0.17
ΔG [kJ.mol^{-1}]	-32.93 ± 0.18
-TΔS[kJ.mol^{-1}]	-48.18 ± 0.24

Figure 16: Isothermal titration calorimetry of inactivated hDPP III with angiotensin-II

Top Left: Evolution of heat over time during the experiment with each peak corresponding to one injection; Bottom Left: Integration of said peaks as a function of hDPP III molar ratio. Right side: Thermodynamic parameters calculated in Origin software (MicroCal)

4. Discussion

hDPP III is an enzyme with promiscuous substrate specificity, which accepts ligands, from tetrapeptides up to decapeptides and hydrolyzes them almost regardless of their amino acid composition. Previous studies on the subject of DPP III suggested a large domain motion upon binding of a ligand molecule, which leads to the upper and lower domain of the enzyme approaching each other and closing the cleft between them [10]. All ligand bound crystal structures we determined were present in said closed conformation. Although we were able to observe hDPP III in complex with natural and synthetic ligands of different lengths and amino acid sequences, the overall conformation of the enzyme does not appear to change significantly depending on the ligand molecule. This can be observed in figure 17, which shows a superposition of six ligand bound DPP III structures determined and analysed during the course of this project. Their respective co-crystallized ligand molecules bound to the active site, are shown superimposed in figure18. The average root means square deviation (RMSD) for Cα atoms was 0.235 Å.

All peptides bind to the conserved five stranded β-sheet on the lower domain in an extended conformation, but the exact mechanism of binding appears to be slightly different in each structure. All structures with the exception of SHE and endomorphin-2 bound hDPP III display an antiparallel binding to the five stranded β-core region. Electron density for the catalytic zinc ion could be observed in all structures, with the exception of angiotensin-II bound hDPP III. However, only peptides with inhibitory effect towards DPP III were observed in a conformation which would allow them to directly interact with the zinc ion.

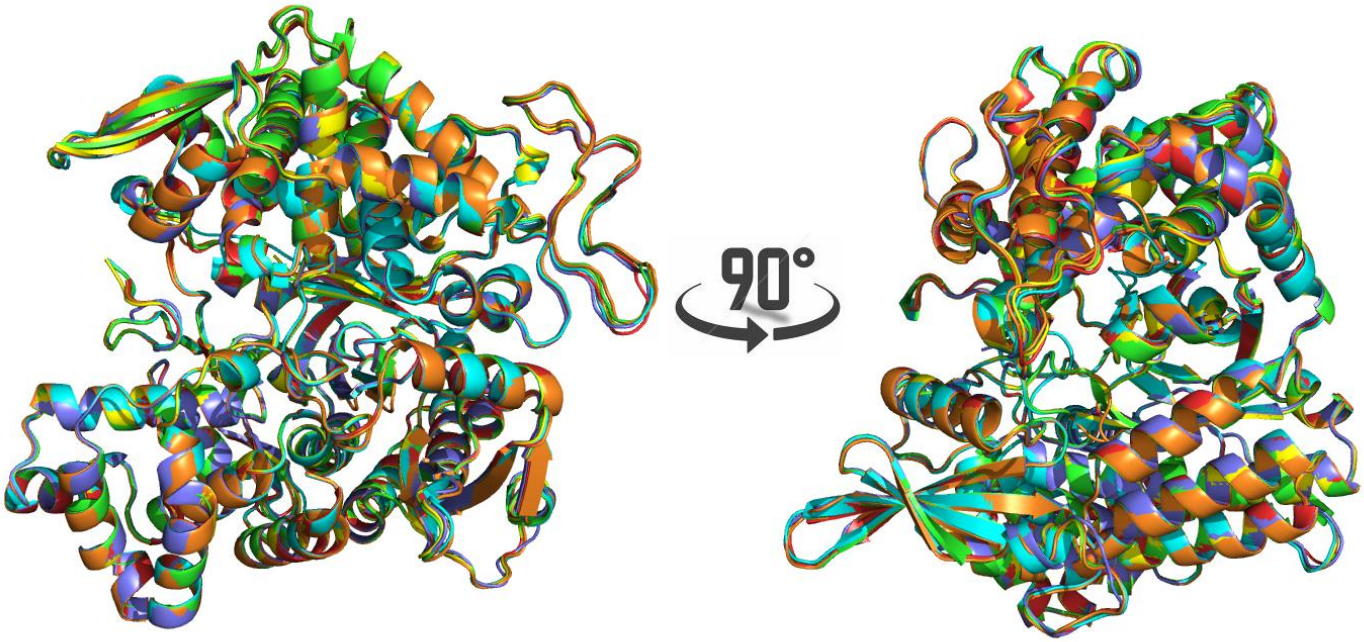

Figure 17: Superposition of six hDPP III structures in complex with different ligands

The structures are coloured as follows: Green: Met-enkephalin; Cyan: Angiotensin-II; Red: Endomorphin-2; Yellow: Leu-enkephalin; Orange: IVYPW; Dark Blue: SHE. The right side picture is rotated by 90°. Figure created in Pymol.

Figue 18 also highlights, that the N-terminal region of the peptide ligands are especially tightly coordinated, while their C-termini are comparatively more flexible. Since DPP III cleaves dipeptides sequentially from the N-terminus of its substrates, it is reasonable to assume that exact positioning of this region is favourable towards effective hydrolysis. This tight coordination of the peptide N-terminus might also explain the enzymes dipeptidase specificity. Even though it accepts a wide variety of ligands, no known side reactions of DPP III have been reported so far, which suggests a high specificity towards dipeptidase activity.

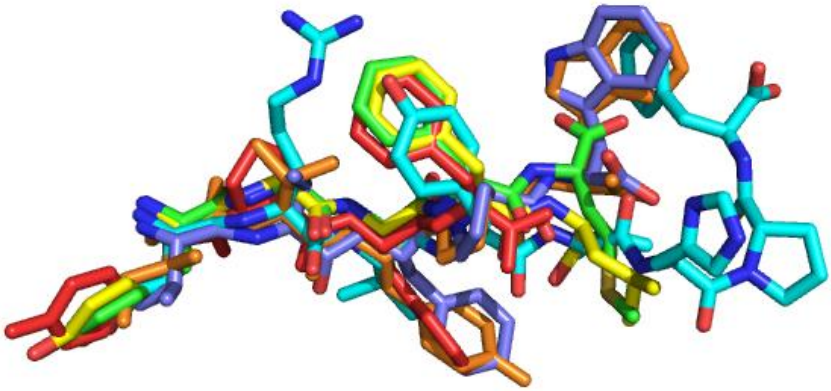

Figure 18: Superposition of the ligand molecules in complex with hDPPPIII

The ligand molecules are coloured as follows: Green: Met-enkephalin; Cyan: Angiotensin-II; Red: Endomorphin-2; Yellow: Leu-enkephalin; Orange: IVYPW; Dark Blue: SHE. N-terminal regions are located on the left side of this figure. Created with Pymol.

The hDPP III constructs used in this study carry point mutations on surface residues, which were originally designed for sm-FRET experiments, in addition to being shortened by 11 amino acids. Unexpectedly, the Cys207 residue only present in these constructs has introduced an intermolecular contact in the form of a disulfide bridge. This disulfide bridge forms between Cys207 and the corresponding Cys207 of a symmetry related hDPP III molecule, as depicted in figure 19. This contact might have provided an additional stabilization, which aided in intermolecular crystal packing and thereby the crystallization process [29].

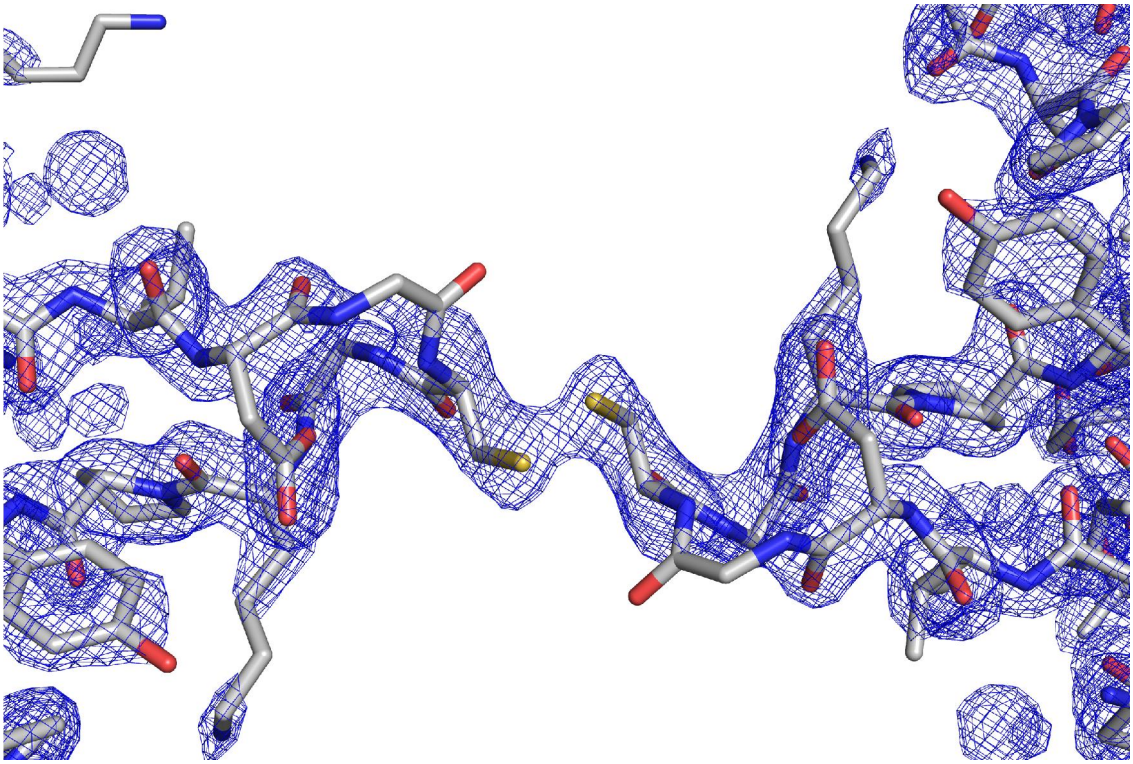

Figure 19: Intermolecular disulfide bridge

Contact formed between Cys207 of two symmetry related hDPP III molecules. Figure reused from [28]

4.1 hDPP III in complex with synthetic inhibitors

IVYPW - Studies by *Chiba et al.* sought to synthesize effective antagonist towards DPP III by utilizing several hemorphin-like pentapeptides [19]. This study revealed, that a tetrapeptide core of VYPW was essential for inhibition of DPP III. Of all peptides tested in the aforementioned study, IVYPW exhibited the strongest inhibition towards rat DPP III. Therefore, crystallizing IVYPW in complex with DPP III could be considered an important step in analysing and understanding its inhibitory properties and thereby providing the foundation for future design of specific DPP III inhibitors. The binding mode of IVYPW proved to be identical to the tynorphin (VVYPW) bound structure, as can be seen in figure 20. Importantly however, The IVYPW bound structure contains electron density for the catalytic zinc ion, which is lacking in tynorphin bound hDPP III.

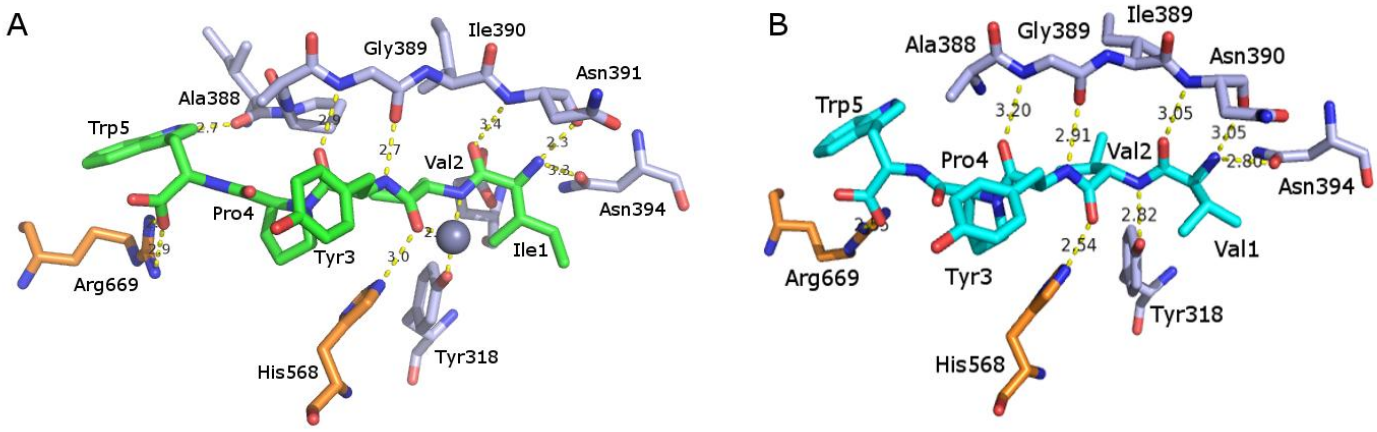

Figure 20: Comparison of IVYPW - and Tynorphin bound DPP III active sites

A: Active site of IVYPW bound hDPP III with the ligand molecule shown in green. The catalytic zinc ion can be seen in this structure as a grey sphere. B: Active site of tynorphin bound hDPP III (PDB Code: 3T6B) with the ligand molecule in cyan. On both sides, residues contributed from the upper domain of the enzyme are shown in orange and residues from the lower domain are shown in light blue. Dashed yellow lines represent interaction distances in Å. Figure created with Pymol.

In previously determined crystal structures of human and yeast DPP III without ligand, coordination of the catalytic zinc ion is achieved with His450 and His455 from the ^{450}*HEXXGH*^{455} sequence and Glu508 from the ^{507}EECRA(E/D)^{512} consensus sequence. In these structures, the tetrahedral coordination of the zinc ion is completed with a conserved water molecule. This led to the proposal, that DPP III operates with a water mediated mechanism, akin to thermolysin and neprilysin, since these two well characterized, zinc dependent metallopeptidases show a very similar coordination [16,17]. In the IVYPW bound structure however, we observed the zinc ion coordinated with the carbonyl oxygen of Val2, instead of a water molecule. This could possibly lead to a different, less effective hydrolytic mechanism, which will be discussed in more detail later in this chapter.

SHE - A different approach for finding an effective inhibitor to DPP III, was employed with the design of the peptidomimetic SHE. By modifying an existing peptide, several of the compounds properties such as stability, bioavailability,

receptor selectivity and potency of enzyme inhibition can be altered. For both IVYPW and SHE, the foundation of their design was the availability of tynorphin bound DPP III, since no crystal structures of specific DPP III inhibitors have previously been reported. By analysing the active site arrangement of tynorphin bound DPP III in a structure based peptidomimetic approach, it was possible to design a compound which mimics the hydrolytic transition state. This improves binding of the synthetic compound to the active site. Additionally, SHE displays a C-C bound between C3 and C4 position instead of a peptide bond. This change was introduced in order to reduce the compounds degradability by hydrolytic activity of dipeptide N-end cutters such as DPP III.

Synthetic peptide ligands such as tynorphin or IVYPW could be considered "bad substrates" rather than inhibitors, since they slowly get hydrolyzed over time. IVYPW and SHE bound structures were determined at resolutions of 2.76 Å and 2.64 Å respectively, which has to be taken into consideration when interpreting these results.

4.2 hDPP III in complex with in vitro substrates

4. 2. 1 hDPP III in complex with Met-enkephalin and Leu-enkephalin

Enkephalins are a group of naturally occuring pentapeptides found in the brain, spinal cord and digestive tract of many animal species, which also includes humans. These bioactive compounds serve as neurotransmitters, as they bind to the δ -opioid receptor, involved in the pain regulatory system [8]. Previous studies on the subject have shown, that enkephalins exhibit an endothermic binding behaviour, and can be effectively hydrolyzed by hDPP III [11]. Because of its affinity to neuroactive peptides such as met-enkephalin and leu-enkephalin, DPP III has previously been characterised as enkephalinase B. The enkephalin compounds used for co-crystallization in this study were met-enkephalin, with an amino acid composition of

Tyr-Gly-Gly-Phe-Met (figure 21) and leu-enkephalin with an amino acid composition of Tyr-Gly-Gly-Phe-Leu (figure 22).

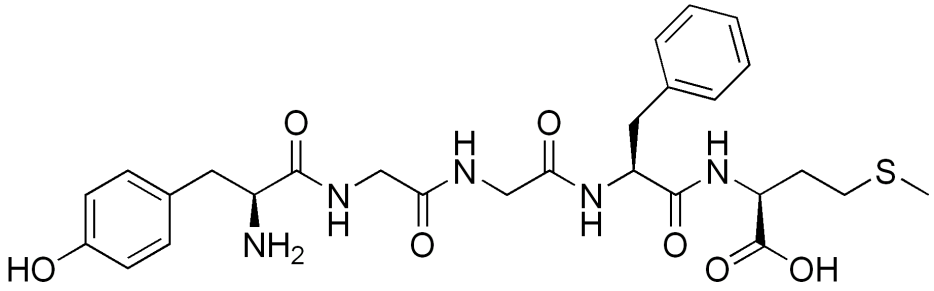

Figure 21: Skeletal formula of met-enkephalin

Endogenous opioid pentapeptide ligand structure. Figure created with Chemdraw software.

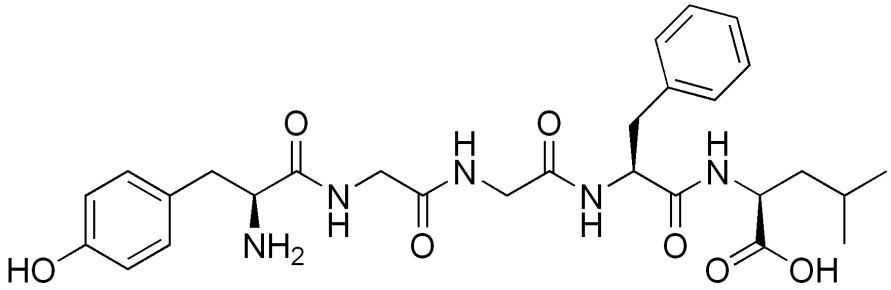

Figure 22: Skeletal formula of leu-enkephalin

Endogenous opioid pentapeptide ligand structure. Figure created with Chemdraw software.

Figure 23 and figure 24 depict a close-up of the met-enkephalin bound an leu-enkephalin bound active sites respectively. As the structure with the highest resolution, met-enkephalin bound DPPII was determined at 1.84 Å, while the structure with leu-enkephalin was determined with a resolution of 2.05 Å. Both structures have been added to the RCSB Protein Data Bank and can be accessed with the codes: 5E33 for met-enkephalin and 5E3A for leu-enkephalin bound hDPP III. The peptides exhibit an extended conformation and bind to the active site in an antiparallel fashion. This is especially noteworthy, since both peptides contain two glycine residues, which are known to disrupt the formation of secondary structures elements, due to their high conformational flexibility. In both cases, a series of hydrogen bond interactions from Ala388 up to Asn391 serves to stabilize the substrates in their extended

conformation. The N-termini of both pentapeptides are also connected to the side chains of Glu316, Tyr318 and Asn394 via hydrogen bonds. There are slight changes in the mode of binding however. Leu-enkephalin shows a connection with Arg572, contributed from the upper lobe of DPP III. This interaction is missing in met-enkephalin, as the corresponding residues are too far apart to allow for the formation of a hydrogen bond. Furthermore, the conserved Arg669 residue, which interacts with the C-terminus of met-enkephalin, most likely via the formation of a salt bridge, shows no interaction towards leu-enkephalin. We observed the catalytic zinc ion present in both enkephalin bound structures. However at a distance of 3.7 Å for met-enkephalin and 3.6 Å for leu-enkephalin from the P1 carbonyl of the peptide, it likely does not interact directly with these two ligands.

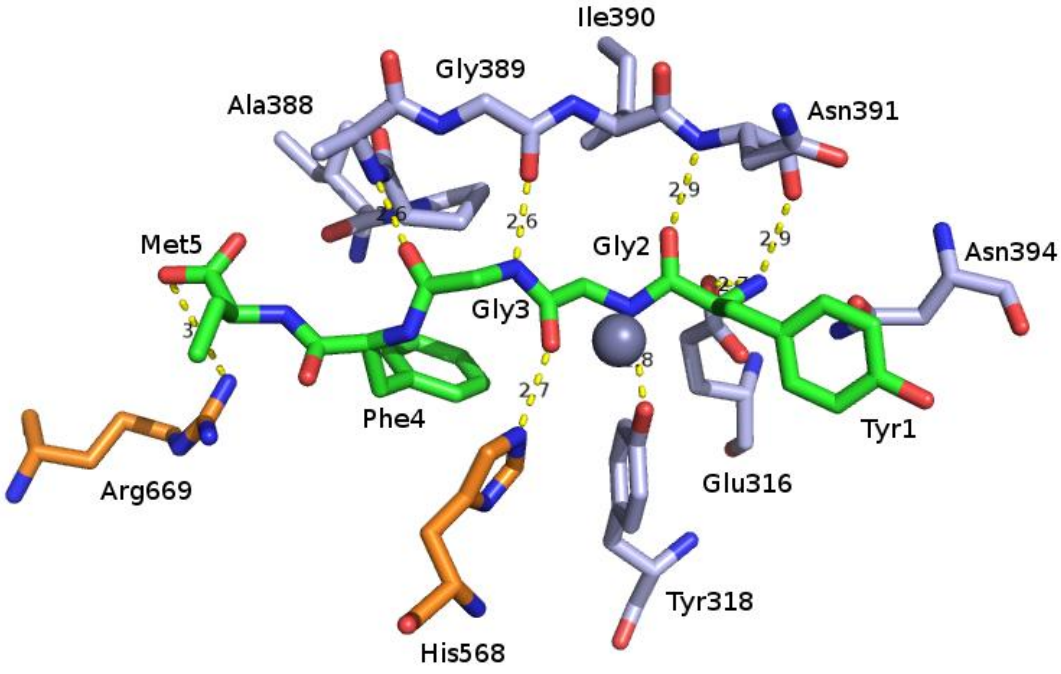

Figure 23: Met-enkephalin bound to hDPP III active site

Residues and interactions involved in binding of met-enkephalin to the hDPP III active site. The ligand molecule is shown in green; Residues contributed from the lower domain of the protein are coloured in light blue; Residues contributed from the upper domain of the protein are coloured in orange; The grey sphere represents the catalytic zinc ion scaled to 50%radius; Dashed yellow lines show interaction distances in Å. Figure drawn in Pymol.

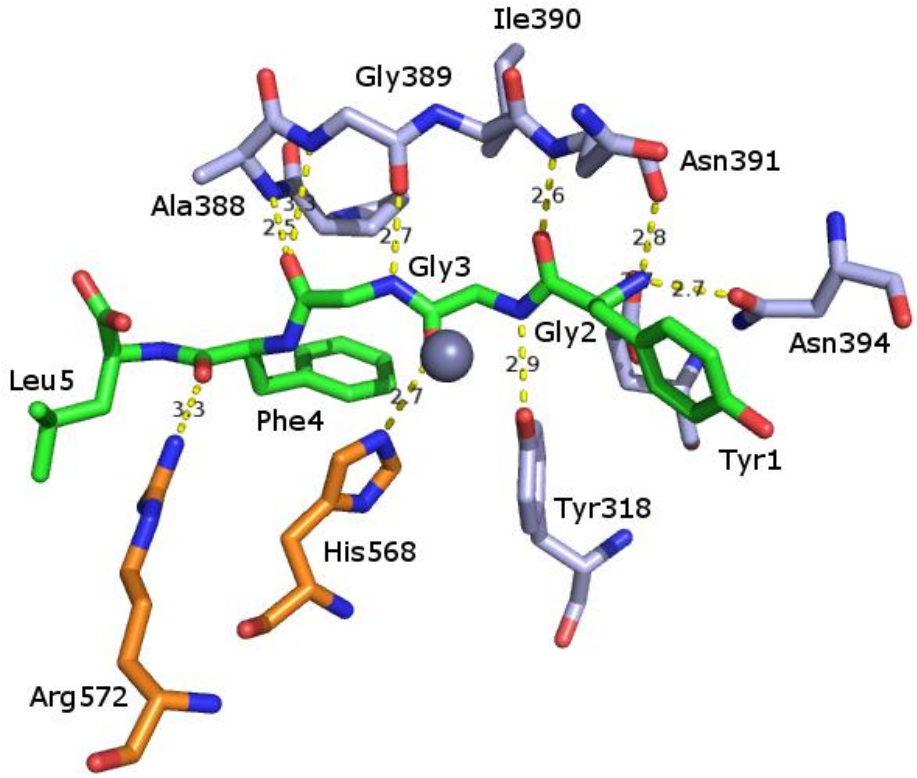

Figure 24: Leu-enkephalin bound to hDPP III active site.

Residues and interactions involved in binding of leu-enkephalin to the hDPP III active site. Leu-enkephalinis shown in green; Residues contributed from the lower domain of the protein are shown in light blue; Residues contributed from the upper domain of the protein are shown in orange; The Grey sphere shows the catalytic zinc ion scaled to 50% radius; Dashed yellow lines are interaction distances in Å. Figure drawn in Pymol.

4. 2. 2 hDPP III in complex with angiotensin-II

Angiotensin-II is an octapeptide with the amino acid composition of Asp-Arg-Val-Tyr-Ile-His-Pro-Phe, as shown in figure 25. This peptide hormone is a metabolite in the renin/angiotensin system (RAS), which is a system involved in blood pressure regulation and fluid balance. It is produced by converting angiotensin-I via the angiotensin converting enzyme (ACE) and has been

indicated as a potent vasoconstrictor [3,19]. Therefore, degradation of angiotensin-II by hDPP III could lead to lowered blood pressure.

ITC experiments have revealed, that angiotensin-II exhibits an entropy driven binding interaction towards hDPP III, similar to peptide ligands observed in previous studies [11]. Entropy driven binding processes tend to be more hydrophobic in character as opposed to enthalpy driven processes which are primarily characterized by hydrogen bonding and van der Waals interactions. The water molecules in the large left between upper and lower domain has been described as an entropy reservoir by *Bezerra et al*. Displacement of these water molecules might be the driving force, which facilitates the large domain motion and subsequent peptide binding. This is a possible explanation for the largely entropy favoured binding observed not only in angiotensin-II, but other peptide ligands such as endomorphin-2, IVYPW and leu-enkephalin as well. ITC also revealed that angiotensin-II binds relatively tightly to hDPP III, with a dissociation constant (K_d) of 1.64 µM.

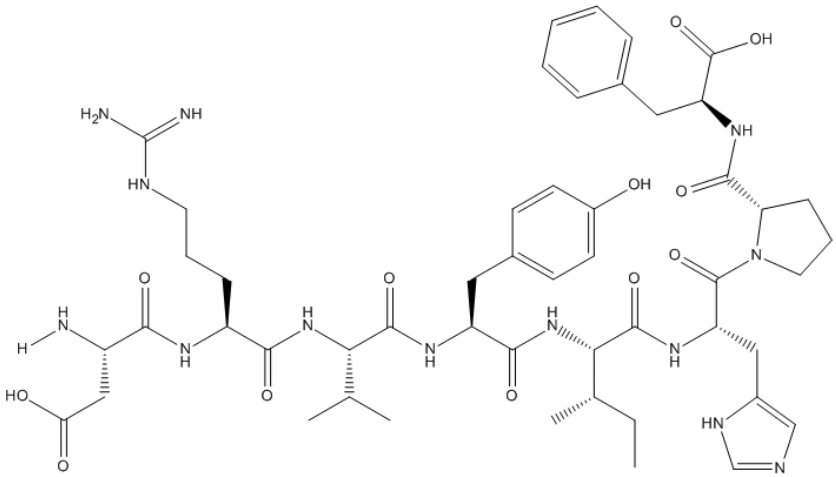

Figure 25: Skeletal formula of angiotensin-II

Octapeptide ligand used in co-crystallization and in complex with inactive DPP III as seeding stock in microseeding experiments . Figure drawn in Chemdraw software.

Since angiotensin-II bound hDPP III was the first structure we were able to successfully crystallize and determine, no seeding stock was availabe prior to this experiment. All further crystallization attempts were carried out using 0.2 µl of seeding stock, created from poorly formed crystals of hDPP III in complex

with angiotensin-II. As a result, the time to produce diffraction quality crystals improved drastically, from two months to within a week. This structure has also been added to the RCSB Protein Dtaa Bank and can be accessed with the code: 5E2Q.

Figure 26 shows a close-up of the catalytic site of hDPP III in complex with angiotensin-II and the residues involved in peptide binding. This structure was determined at a resolution of 2.40 Å We observe the formation of a cis-peptide bond between His6 and Pro7 of angiotensin-II, which forces the larger molecule to make a turn, thereby effectively adapting to the active site constraints of hDPP III. Previous studies have shown, that angiotensin-II in aqueous solutions can form cis-peptide turns along its backbone structure [30]. Extensive hydrogen bond interactions firmly anchor the peptide in the active site. Stabilisation of the peptides N-terminus is achieved via polar contact to the side chains of Glu316, Tyr318 as well as Asn394. Asp1 of the peptide interacts with a nitrogen atom of His455, which is located on the conserved ^{450}HEXXGH^{455} zinc binding motif. We did not observe an electron density for the catalytic zinc ion in this structure. It is probable, that the zinc atom was sequestered over time, since in this particular case the crystal was grown for approximately two months in a phosphate containing buffer. Prolonged exposure to phosphate buffers leads to sequestration of divalent cations.

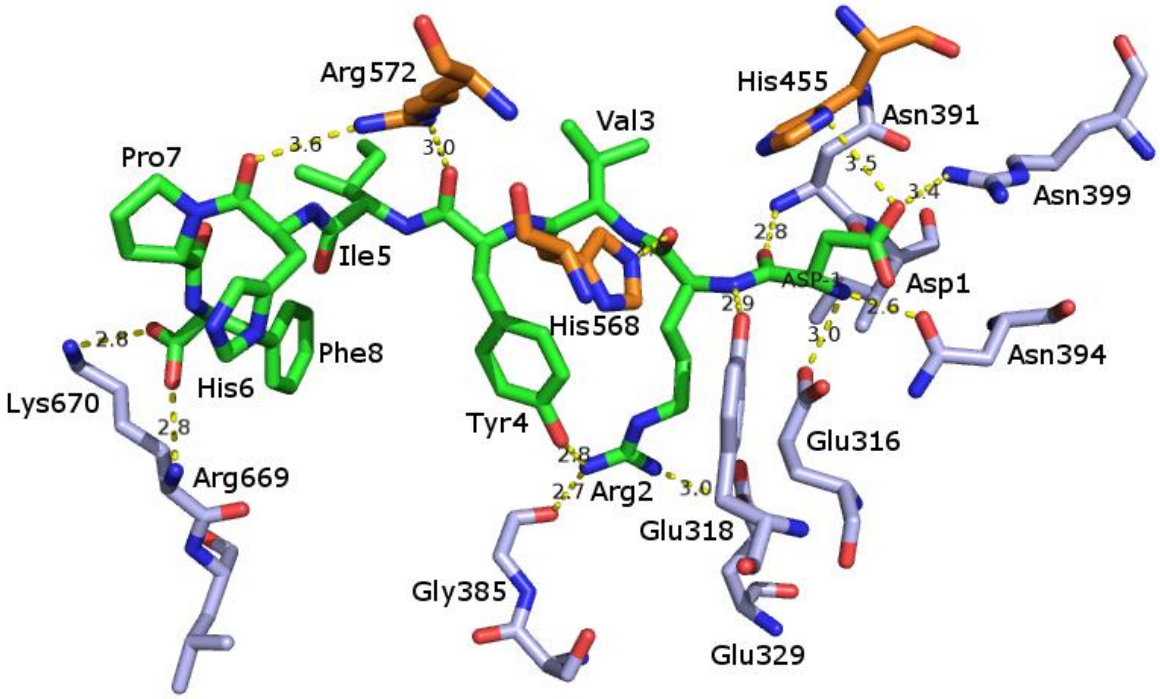

Figure 26: Angiotensin-II bound to hDPP III active site

Residues and interactions involved in binding of angiotensin-II to the hDPP III active site. The ligand molecule is shown in green; Residues contributed from the lower domain of the protein are shown in light blue; Residues contributed from the upper domain of the protein are shown in orange; Dashed yellow lines show interaction distances in Å. Figure drawn in Pymol.

4. 2. 3 hDPP III in complex with endomorphin-2

Endomorphins are a group of opioid peptides, which bind to the μ-opioid receptor with high affinity and selectivity [31]. Endomorphin-2, a tetrapeptide with the amino acid sequence of Tyr-Pro-Phe-Phe-NH_2 ,as pictured in figure 27, has been shown to induce the release of dynorphin A and met-enkephalin in the spinal cord and lower brain stem [2]. Furthermore, endomorphin-2 is the only tetrapeptide, and simultaneously the shortest ligand we were able to co-crystallize in complex with hDPP III. The crystal structure of hDPP III in complex with endomorphin-2 has been added to the RCSB Protein Data Bank and can be accessed with the code: 5EHH.

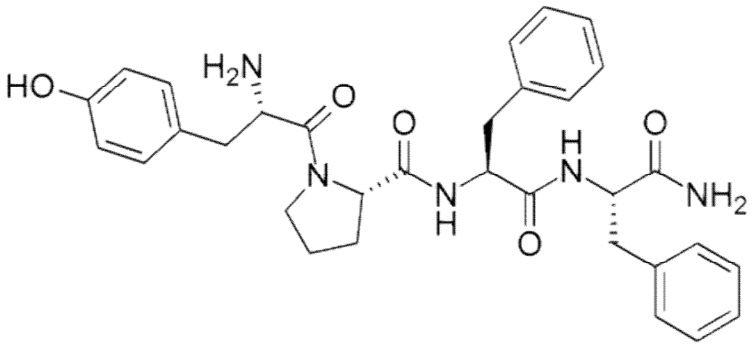

Figure 27: Skeletal formula of endomorphin-2

Endogenous opioid peptide ligand. Amidation at the C-terminus. Figure created with Chemdraw.

The active site residues of hDPP III in complex with endomorphin-2 can be seen in figure 28. This crystal structure was determined with a resolution of 2.38 Å. It is important to point out that endomorphin-2 features a proline residue at the second position from the N-terminus, because proline residues are known to serve as β-strand breakers, which would explain why endomorphin-2 does not form a β-strand in the active site region. Furthermore, this proline residues makes endomorphin-2 resistant to cleavage from some dipeptidases. However, kinetic data has shown that DPP III is able to work as a post proline cleaving enzyme, as exhibited by its ability to hydrolyze endomorphin-1 [8]. Although no kinetic data for hydrolysis of endomorphin-2 are currently available, similar results are to be expected, since the structure only diverges from endomorphin-1 by one residue. In this structure, residues from both the upper domain and the lower domain contribute in binding of the ligand. The hydrogen bond network from Ala388 up to Asn391, which is also present in other DPP III structures, can be observed here as well. The N-terminus of the peptide is anchored with polar interactions provided by Asn 394 and Arg399. Although tyrosine is also the first N-terminal residue in the met-enkephalin and leu-enkephalin bound structures, this interaction with Arg399 was not observed in these two structures. Furthermore, Tyr318 does not interact with endomorphin-2, because of the proline residue at the second position. The catalytic zinc ion can be observed in contact with the Pro2 of the peptide.

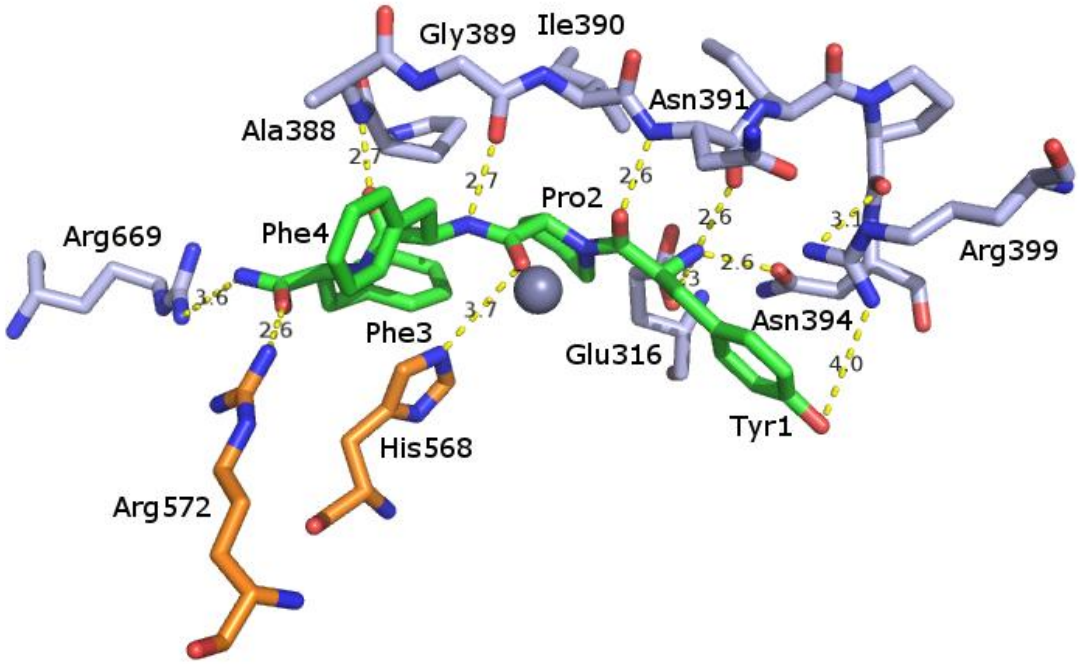

Figure 28: Endomorphin-2 bound to hDPP III active site

Residues and interactions involved in binding of endomorphin-2 to the hDPP III active site. Endomorphin-2 is shown in green; Residues contributed from the lower domain of the protein are shown in light blue; Residues contributed from the upper domain of the protein are shown in orange; The grey sphere represents the catalytic zinc ion scaled to 50% radius ; Dashed yellow lines represent interaction distances in Å. Figure drawn in Pymol.

4.3 Anion - aromatic interaction

An anion - aromatic interaction, or anion - π interaction, is an attractive force between a negatively charged group and the positively charged ring edge of an electron-deficient aromatic system. This noncovalent bond is energetically weaker when compared to the related, more thoroughly researched cation- π interaction, but its potential structural and functional importance should not be discarded. Noncovalent interactions involving aromatic side chains such as phenlyalanine, tyrosine and tryptophane can help to improve protein-ligand binding, as well as protein structure formation and stability [21].

A study conducted by *Schwans et al.* suggested, that anion-aromatic interactions can facilitate the positioning of a general acid or base in an enzymes active site. For this purpose, phenylealanine residues display a selective advantage when compared to hydrogen bonding groups, since they can facilitate the binding of hydrophobic substrates as well [20]. *Schwans et al* illustrated this interaction with the positioning of a general base in the active site of a ketosteroid isomerase from *Camomonas testosteroni*.

In the case of DPP III, we considered a possible anion - aromatic interaction between the conserved Phe373 residue and the catalytically important Glu451 residue, situated at the ^{450}HEXXGH^{455} zinc binding motif. This potential interaction is illustrated by figure 29, which was created using the ligand free version of hDPP III in its open conformation (PDB code: 3FVY) The crystal structures solved in this study could not be used in figure 29, since they invariably carry the E451A mutation.

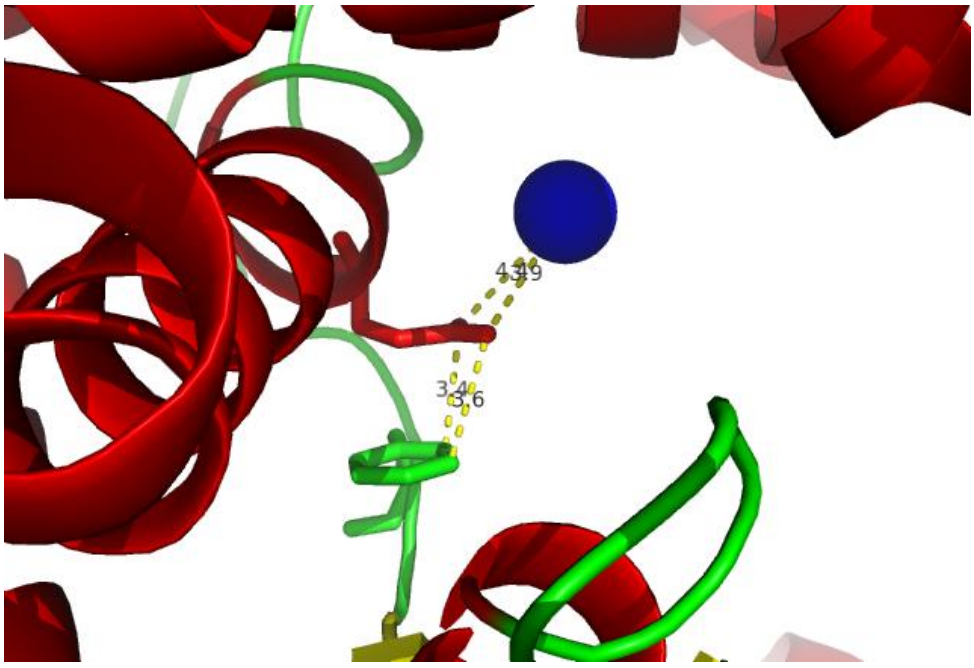

Figure 29: Potential anion-aromatic interaction

Interaction between the catalytic Glu451 and the aromatic ring system of Phe373. Residues shown in red are part of an α-helix, residues shown in green are part of a loop region. The zinc ion is shown as a blue sphere. Yellow dashed lines represent interaction distances. Figure was created in Pymol, with the open unbound hDPP III structure as a model (PDB Code: 3FVY)

In order to confirm this suspected interaction, fluorescent activity assays were carried out, using wt DPP III as well as the F373L variant of hDPP III. This F373L variant is catalytically active, but abolishes the possible anion - aromatic interaction by exchanging the aromatic phenylalanine with a leucine residue.

When performing these activity assays, we found that DPP III degrades quickly, even when constantly kept on ice and under the exclusion of light. To alleviate this problem, which led to losses in expected catalytic activity, fresh protein stock solutions were prepared in regular intervals. While the michaelis menten constant K_M did not change between the two tested DPP III variants, the turnover number K_{cat} is more then 20 times lower in F373L DPP III. This significant reduction in catalytic activity confirms that Phe373 is noncovalently bonded to Glu451 and that this interaction is important for effective hydrolysis.[20].

4.4 Proposed mechanism of catalysis

As mentioned previously, tynorphin, IVYPW and SHE might be considered "bad substrates" rather than inhibitors, since they get hydrolyzed by DPP III, but very slowly and therefore inefficiently. When compared to more effectively hydrolyzed compounds such as the enkephalins, we observed a different mode of binding to the catalytic zinc ion, which might be the key difference between substrate bound structures and inhibitor bound structures. In the previously determined unbound structure of yeast and human DPP III, as well as most substrate bound structures determined in this study, a conserved water molecule completes the tetrahedral geometry of the zinc ion. In the slow substrate/inhibitor bound structures on the other hand, the zinc ion can be observed in direct contact with the ligand molecule instead.

Tetrahedral coordination is achieved either with the Val2 residue in both tynorphin and IVYPW, or the C_4 carbon of hydroxyethylene in SHE. Due to this direct contact between the ligand and the zinc ion, the water molecule is displaced. A comparison between zinc binding coordination of substrates, represented by met-enkephalin bound hDPP III and inhibitors represented by IVYPW bound hDPP III is illustrated in figure 30.

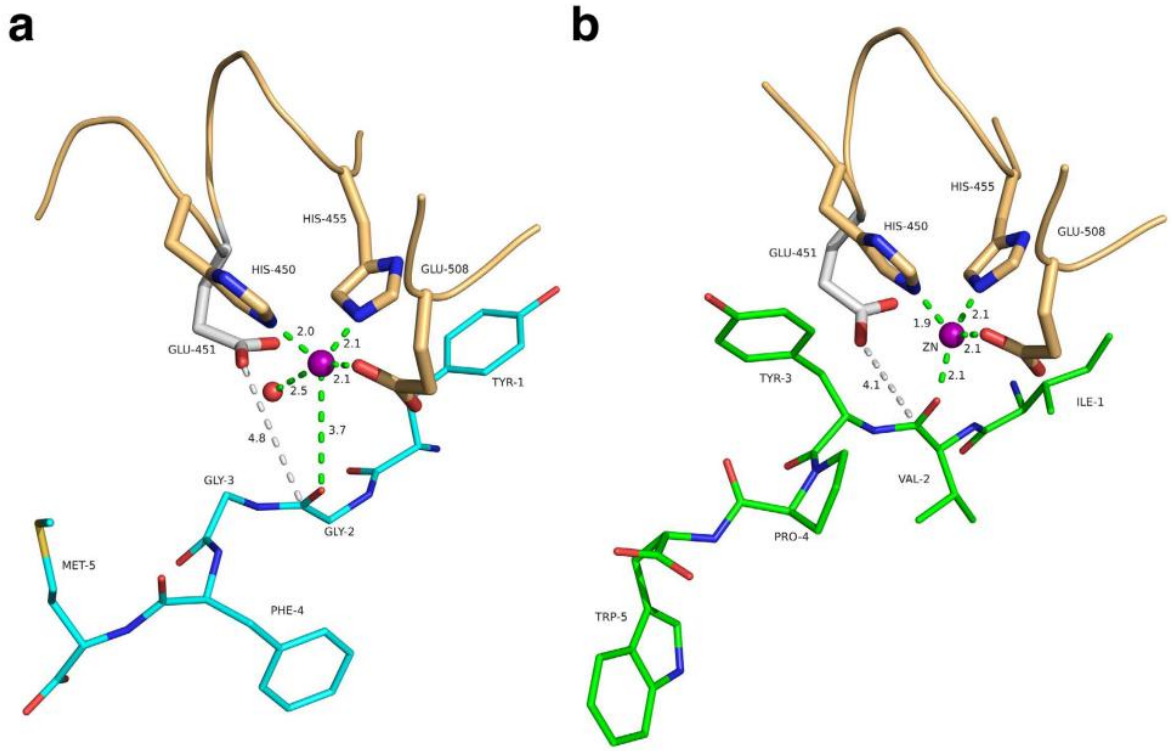

Figure 30: Comparing substrates and inhibitors regarding coordination of the catalytic zinc ion

A: Residues involved in zinc ion coordination in met-enkephalin bound hDPP III, ligand molecule shown in cyan; B: Residues involved in zinc coordination in IVYPW bound hDPP III, ligand molecule is shown in green; Both structures: Zinc ion coordinating residues shown in gold; Glu451, which was modelled in COOT based on the open, unbound structure of hDPP III (PDB: 3FVY) is shown in white. Dashed lines represent interaction distances, The zinc ion is depicted as a purple sphere. The conserved water molecule is presented as a red sphere. This figure was reused from [28].

Since these complexes were obtained with the inactive hDPP III variant, the catalytic Glu451 residue had to be modelled in COOT. There are exceptions to this observation however, in the form of angiotensin-II and endomorpin-2. For endomorphin-2 bound hDPP III, we observed the catalytic zinc ion in contact with the Pro2 residue of the peptide, even though endomorphin-2 is not considered an inhibitor of DPP III. The electron density for endomorphn-2 was not well defined at the C-terminus and the center of the molecule. The occupancy for this ligand molecule had to be reduced, as it was less than 100%. In the case of angiotensin-II, we were not able to observe electron density for the catalytic zinc ion as it most likely got sequestered due to prolonged exposure in phosphate containing buffer.

The binding coordination shown on the left side of figure 30 is very similar to well researched zinc dependent metallopeptidases such as neprilysin and thermolysin, as *Baral et al.* have pointed out when researching yeast DPP III [10]. They proposed, that accordingly, hDPP III might employ a similar mechnism of hydrolysis.

Figure 31 depicts this proposed water mediated hydrolytic pathway for substrate bound structures at the top, and the proposed anhydride pathway for inhibitor bound structures on the bottom. In the water mediated pathway, the Glu451 residue serves as a general base and deprotonates a conserved water molecule, which is in contact with the zinc ion. This increases the waters nucleophilicity and enables it to attack the ligand molecules carbonyl carbon at the scissile peptide bond. Thereby, a tetrahedral transition state is formed, with the carbonyl oxygen now completing the tetrahedral zinc ion coordination. This oxyanion transition state is stabilized by interaction with the conserved His568. When the leaving nitrogen group is protonated by the side chain of Glu451, the intermediate collapses and the cleaved dipeptide leaves the active site.

In the inhibitor bound structures, represented by IVYPW bound hDPP III in figure 30, the zinc ion is in direct contact with the backbone carbonyl group of the Val2 residue instead. The ligand is much closer to the zinc ion, which leaves no space for a water molecule. Accordingly, these structures have to employ a different catalytic mechanism [18]. As depicted at the right side of figure 30, the carboxylate side chain of Glu451 could act as nucleophile, by attacking the carbonyl carbon of the scissile peptide bond directly. Instead of an oxyanion transition state, this would lead to the formation of an acyl-enzyme intermediate, as depicted at the bottom half of figure 31. The transition state is broken, when the Glu451 side chain is subsequently hydrolyzed by water. This pathway shows similarities with the anhydride pathway which was proposed for Carboxypeptidase A (CPA), which is another zinc dependent enzyme which bares similarities to the hDPP III active site conformation [18, 32].

When compared to the promoted-water pathway, the deacylation step present only in the anhydride pathway is energetically less favorable, which might explain why the corresponding ligand molecules are considered bad substrates or even inhibitors of hDPP III [18].

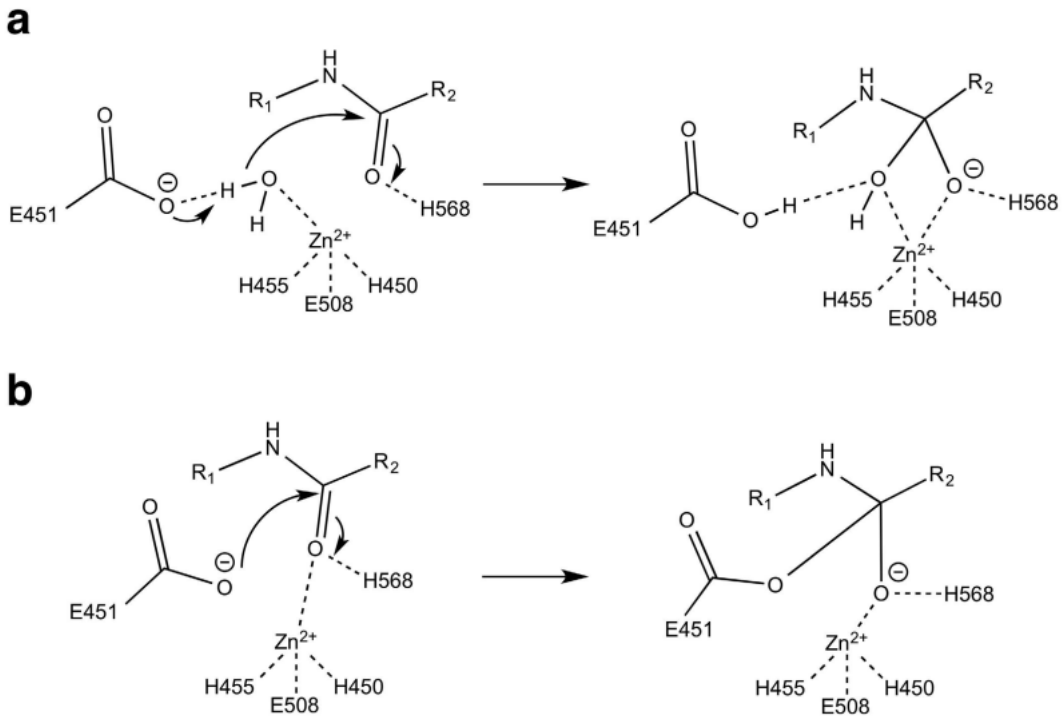

Figure 31: Proposed mechanisms of catalysis

A: Representation of the promoted-water pathway, using a deprotonated water molecule to attack the scissile peptide bond. B: Representation of the anhydride pathway, with the side chain of a glutamate residue directly initiating a nucleophilic attack at the scissile peptide bond. Figure reused from [28].

4.5 Conclusions

The crystal structures determined and analysed over the course of this project hopefully serve to broaden the general knowledge on the subject of DPP III, as well as its possible future applications. We were able to obtain high resolution structures of hDPP III in complex with compounds that are considered to be natural substrates of the enzyme.

All structures have been determined with their co-crystallized ligand bound in the enzymes active site and they all displayed a closed overall conformation. This overall conformation does not seem to change depending on the type of ligand bound, however the exact mode of binding is subtly different in each structure. In most complexes, we found that the ligand binds as a β-strand to the 5-standed sheet on the enzymes lower domain. This maximizes the number of possible hydrogen bonding interactions.

This is also the first time that hDPP III has been crystallized in complex with specifically designed synthetic inhibitors. Due to these inhibitor bound structures we learned, that the main difference between substrates and "bad substrates" or inhibitors of DPP III might lie in the tetrahedral coordination of the catalytic zinc ion. In substrate bound structures, the tetrahedral coordination is completed by a conserved water molecule, which might enable the enzyme to utilize a water-promoted hydrolytic pathway. In the inhibitor bound structures on the other hand, the ligand molecule was observed in direct interaction with the zinc ion and the conserved water molecule is displaced. In these structures, the enzyme likely utilizes an energetically less favourable anhydride pathway.

Typically, the specificity of a peptidase is characterized by the substrates amino acid composition around the scissile bond [2]. It is still unclear, why DPP III is inhibited by compounds such as IVYPW or tynorphin, while other compounds with similar length and amino acid composition get cleaved efficiently. Our findings suggest, that ligand molecules such as IVYPW or tynorphin force the catalytic reaction down the anhydride pathway. This would

help to explain, why these bad substrate ligands can inhibit DPP III, but still get hydrolyzed slowly over time.

The electron density for the ligand molecules was consistently well defined at their N-terminal regions. Since DPP III is characterized by its N-terminal exopeptidase activity, tight coordination of the ligand molecules at this region is important for effective hydrolysis. The C-terminal end appears to be more flexible.

We suspected the presence of an anion-aromatic interaction, which would serve to correctly position the catalytically essential residue Glu451 in the active site. This interaction could be confirmed via fluorescent activity assays, performed with wt DPP III and F373L DPP III. The F373L mutant, which cannot utilize this anion-aromatic interaction, exhibited a 20 fold reduction in catalytic activity, when compared to the wild type enzyme.

List of figures

Figure 1: Comparison of open and closed conformation of human DPP III 8
Figure 2: SDS-PAGE after affinity chromatography of inactive hDPP III..... 20
Figure 3: SDS-PAGE after reverse affinity chromatography of inactive hDPP III 21
Figure 4: SDS-PAGE after anion exchange chromatography of inactive hDPP III 22
Figure 5: SDS-PAGE after size exclusion chromatography of inactive hDPP III 22
Figure 6: Crystal morphology of inactive hDPP III in complex with leu-enkephalin 24
Figure 7: Skeletal formula of IVYPW 26
Figure 8: Overall structure of hDPP III in complex with IVYPW 27
Figure 9: IVYPW bound to hDPPII active site 28
Figure 10: Electron density maps for the IVYPW ligand molecule 29
Figure 11: Skeletal formula of synthetic inhibitor (S)-hydroxyethylene 30
Figure 12: Overall structure of hDPP III in complex with SHE 31
Figure 13: SHE bound to hDPPII active site 32
Figure 14: Electron density maps for the SHE ligand molecule 32
Figure 15: Fluorescent activity assays with wt DPP III and F373L DPP III..... 33
Figure 16: Isothermal titration calorimetry of inactivated hDPP III with angiotensin-II 35
Figure 17: Superposition of six hDPP III structures in complex with different ligands 37
Figure 18: Superposition of the ligand molecules in complex with hDPPPIII.. 38
Figure 19: Intermolecular disulfide bridge 39
Figure 20: Comparison of IVYPW - and Tynorphin bound DPP III active sites 40
Figure 21: Skeletal formula of met-enkephalin 42
Figure 22: Skeletal formula of leu-enkephalin 42
Figure 23: Met-enkephalin bound to hDPP III active site 43
Figure 24: Leu-enkephalin bound to hDPP III active site. 44
Figure 25: Skeletal formula of angiotensin-II 45

Figure 26: Angiotensin-II bound to hDPP III active site 47
Figure 27: Skeletal formula of endomorphin-2..... 48
Figure 28: Endomorphin-2 bound to hDPP III active site..... 49
Figure 29: Potential anion-aromatic interaction..... 50
Figure 30: Comparing substrates and inhibitors regarding coordination of the catalytic zinc ion 52
Figure 31: Proposed mechanisms of catalysis..... 55

5. List of tables

Table 1: Forward and Reverse Primer for site-directed mutagenesis of all DPP III variants 12
Table 2: Thermocycler program for PCR used in site-directed mutagenesis... 12
Table 3: Buffer composition of Zn chelating agents, added during dialysis of DPP III..... 15
Table 4: Crystal parameters and refinement statistics of hDPP III in complex with the inhibitor peptides IVYPW and SHE. Values in parentheses represent the highest resolution shell. 25
Table 5: Comparison of michaelis menten kinetics parameters for both wt DPP III and F373L DPP III variants, used in fluorescent activity assays 34

6. References

1. Rawlings ND, Morton FR, Kok CY, Kong J, Barrett AJ (2008) MEROPS: the peptidase database. Nucleic acids research 36 (Database issue):D320-325.

2. Prajapati SC, Chauhan SS (2011) Dipeptidyl peptidase III: a multifaceted oligopeptide N-end cutter. The FEBS journal 278 (18): 3256–3276.

3. Lee CM & Snyder SH (1982) Dipeptidyl-aminopeptidase III of rat brain. Selective affinity for enkephalin and angiotensin. J Biol Chem 257, 12043–12050.

4. Krissinel, E. & Henrick, K. Inference of macromolecular assemblies from crystalline state. J.Mol.Biol: 372,774–797(2007)

5. Sato H, Kimura K, Yamamoto Y & Hazato T (2003) Activity of DPP III in human cerebrospinal fluid derived from patients with pain. Masui 52, 257–263.

6. 7. Viazzi F, Leoncini G, Pontremoli R. Antihypertensive treatment and renal protection: The role of drugs inhibiting the renin-angiotensin-aldosterone system. High Blood Press Cardiovasc Prev. 2013 Dec;20(4):273–82.

7. Jajčanin-Jozić N, Tomić S, Abramić M.: Importance of the three basic residues in the vicinity of the zinc-binding motifs for the activity of the yeast dipeptidyl peptidase III. J Biochem. 2014 Jan;155(1):43–50.

8. Barsun M, Jajcanin N, Vukelić B, Spoljarić J, Abramić M. Human dipeptidyl peptidase III acts as a post-proline-cleaving enzyme on endomorphins. Biol Chem. 2007 Mar;388(3):343–8.

9.Simaga S, Babić D, Osmak M, Sprem M, Abramić M.: Tumor cytosol dipeptidyl peptidase III activity is increased with histological aggressiveness of ovarian primary carcinomas. Gynecol Oncol. 2003 Oct;91(1):194–200.

10. Baral PK, Jajcanin-Jozić N, Deller S, Macheroux P, Abramić M, Gruber K. The first structure of dipeptidyl-peptidase III provides insight into the catalytic mechanism and mode of substrate binding.J Biol Chem 2008 Aug8 ;283(32):22316-24.

11. Bezerra GA, Dobrovetsky E, Viertlmayr R, Dong A, Binter A, Abramic M, etal. Entropy-driven binding of opioid peptides induces a large domain motion in human dipeptidyl peptidase III. Proc Natl Acad Sci USA. 2012 Apr24;109(17):6525–30.

12. Fukasawa K, Fukasawa KM, Iwamoto H, Hirose J, Harada M. The HELLGH motif of rat liver dipeptidyl peptidase III is involved in zinc coordination andthe catalytic activity of the enzyme. Biochemistry. 1999 Jun 29;38(26):8299–8303.

13. Hooper NM (1994) Families of zinc metalloproteases. FEBS letters 354 (1): 1–6.

14. Yamamoto Y, Hashimoto J, Shimamura M, Yamaguchi T, Hazato T. Characterization of tynorphin, a potent endogenous inhibitor of dipeptidyl peptidaseIII. Peptides. 2000 Apr;21(4):503–8.

15. Rawlings ND, Barrett AJ, Bateman A (2010) MEROPS: the peptidase database. Nucleic acids research 38 (Database issue): D227-33.

16. Jongeneel CV, Bouvier J, Bairoch A (1989) A unique signature identifies a family of zinc-dependent metallopeptidases. FEBS letters 242 (2): 211–214

17. Titani K, Hermodson MA, Ericsson LH, Walsh KA, Neurath H (1972) Amino acid sequence of thermolysin. Isolation and characterization of the fragments obtained by cleavage with cyanogen bromide. Biochemistry 11 (13): 2427–2435.

18. Xu D, Guo H (2009) Quantum mechanical/molecular mechanical and density functional theory studies of a prototypical zinc peptidase (carboxypeptidase A) suggest a general acid-general base mechanism. Journal of the American Chemical Society 131 (28): 9780–9788.

19. Chiba T, Li Y-H, Yamane T, Ogikubo O, Fukuoka M, Arai R, et al. Inhibition of recombinant dipeptidyl peptidase III by synthetic hemorphin-like peptides Peptides. 2003 May;24(5):773–8.

20. Schwans JP, Sunden F, Lassila JK, Gonzalez A, Tsai Y, Herschlag D. Use of anion-aromatic interactions to position the general base in the

ketosteroidisomerase active site. Proc Natl Acad Sci USA. 2013 Jul 9;110(28):11308–13.

21. Frontera A, Gamez P, Mascal M, Mooibroek TJ, Reedijk J. Putting anion-π interactions into perspective. Angew Chem Int Ed Engl. 2011 Oct4;50(41):9564–83.

22. Newman J. Novel buffer systems for macromolecular crystallization. Acta Crystallogr D Biol Crystallogr. 2004 Mar;60(Pt 3):610–2.

23. Kabsch W (2010) XDS. Acta crystallographica. Section D, Biological crystallography 66 (Pt 2): 125–132

24. McCoy, A. J. et al. Phaser crystallographic software. J. Appl. Crystallogr. 40, 658–674 (2007).

25. Adams, P. D. et al. PHENIX: a comprehensive Python-based system for macromolecular structure solution. Acta crystallogr. D 66,213–221 (2010).

26. Emsley, P. & Cowtan, K. Coot: model-building tools for molecular graphics. Acta crystallogr. D 60, 2126–2132 (2004).

27. London, N., Movshovitz-Attias, D. & Schueler-Furman, O. The structural basis of peptide-protein binding strategies. Structure 18, 188–199 (2010).

28. Kumar P, Reithofer V, Reisinger M, Wallner S, Pavkov-Keller T, Macheroux P, et al. Substrate complexes of human dipeptidyl peptidase III reveal the mechanism of enzyme inhibition. Scientific Reports. 2016 Mar 30;6:23787.

29. Compton JR, Legler PM, Clingan BV, Olson MA, Millard CB, Introduction of a Disulfide Bond Leads to Stabilization and Crystallization of a Ricin Immunogen. Proteins. 2011 April ; 79(4): 1048–1060

30. Carpenter KA, Wilkes BC, Schiller PW (1998) The octapeptide angiotensin-II adopts a well-defined structure in a phospholipid environment. European journal of biochemistry / FEBS 251 (1-2): 448–453.

31. Horvath, G. Endomorphin-1 and endomorphin-2: pharmacology of the selective endogenous mu-opioid receptor agonists. Pharmacol. Therapeut. 88, 437–463 (2000).

32 Lee, H. C., Ko, Y. H., Baek, S. B. & Kim, D. H. Detection of an anhydride intermediate in the carboxypeptidase A catalyzed hydrolysis of a peptide substrate by solid state NMR spectroscopy and its mechanistic implication. Bioorg. Med. Chem. Lett. 8, 3379–3384 (1998).

33. Burkard TR, Planyavsky M, Kaupe I, Breitwieser FP, Bürckstümmer T et al. (2011) Initial characterization of the human central proteome. BMC systems biology 5: 17.

34. Vagner J, Qu H, Hruby VJ (2008) Peptidomimetics, a synthetic tool of drug discovery. Current opinion in chemical biology 12 (3): 292–296.